AD-A181 678 AIRCRAFT DYNAMIC RESPONSE TO DAMAGED AND REPAIRED RUNWAYS(U) ADVISORY GROUP FOR AEROSPACE RESEARCH AND DEVELOPMENT NEUILLY-SUR-SEINE (FRANCE) MAR 87 1/1

UNCLASSIFIED AGARD-R-739 F/G 20/14 NL

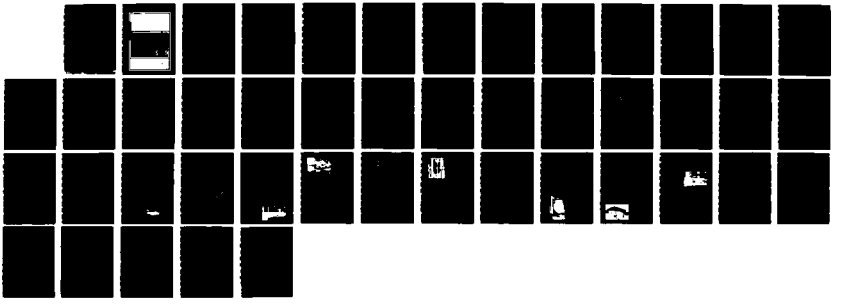

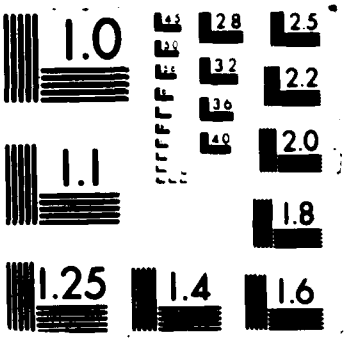
1.0
1.1
1.25
1.4
1.6
1.8
2.0
2.2
2.5
2.8
3.2
3.6
4.0

AGARD-R-739

AGARD-R-739

AGARD

ADVISORY GROUP FOR AEROSPACE RESEARCH & DEVELOPMENT

7 RUE ANCELLE 92200 NEUILLY SUR SEINE FRANCE

AGARD REPORT No.739

Aircraft Dynamic Response to Damaged and Repaired Runways

NORTH ATLANTIC TREATY ORGANIZATION

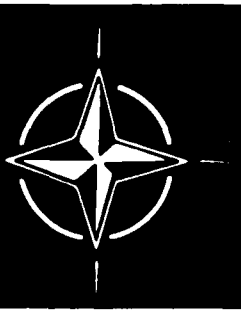

DISTRIBUTION AND AVAILABILITY ON BACK COVER

AGARD-R-739

NORTH ATLANTIC TREATY ORGANIZATION

ADVISORY GROUP FOR AEROSPACE RESEARCH AND DEVELOPMENT

(ORGANISATION DU TRAITE DE L'ATLANTIQUE NORD)

AGARD Report No.739

AIRCRAFT DYNAMIC RESPONSE TO DAMAGED AND REPAIRED RUNWAYS

Papers presented at the 61st Meeting of the Structures and Materials Panel of AGARD in Oberammergau, Germany, 8—13 September 1985.

THE MISSION OF AGARD

The mission of AGARD is to bring together the leading personalities of the NATO nations in the fields of science and technology relating to aerospace for the following purposes:

- Exchanging of scientific and technical information;
- Continuously stimulating advances in the aerospace sciences relevant to strengthening the common defence posture;
- Improving the co-operation among member nations in aerospace research and development;
- Providing scientific and technical advice and assistance to the Military Committee in the field of aerospace research and development (with particular regard to its military application);
- Rendering scientific and technical assistance, as requested, to other NATO bodies and to member nations in connection with research and development problems in the aerospace field;
- Providing assistance to member nations for the purpose of increasing their scientific and technical potential;
- Recommending effective ways for the member nations to use their research and development capabilities for the common benefit of the NATO community.

The highest authority within AGARD is the National Delegates Board consisting of officially appointed senior representatives from each member nation. The mission of AGARD is carried out through the Panels which are composed of experts appointed by the National Delegates, the Consultant and Exchange Programme and the Aerospace Applications Studies Programme. The results of AGARD work are reported to the member nations and the NATO Authorities through the AGARD series of publications of which this is one.

Participation in AGARD activities is by invitation only and is normally limited to citizens of the NATO nations.

Published March 1987

ISBN 92-835-0409-7

Printed by Specialised Printing Services Limited
40 Chigwell Lane, Loughton, Essex IG10 3TZ

ABSTRACT

This report contains two papers on the dynamic response of aircraft operating from damaged and repaired runways. In the first paper the response of a simplified representation of an aircraft to two discrete disturbances is analysed to see how the second disturbance modifies system behaviour caused by the first disturbance. The second paper provides a mathematical model which can be used for calculation of the dynamic response of aircraft structures operating on rough surfaces; a comparison is made between theoretical predictions for a YF16 aircraft and typical measurements from frequency response tests.

RESUME

Deux rapports sont inclus dans cette publication qui traite de la Réponse Dynamique d'un avion opérant sur Piste Endommagée et Reparée. Dans le premier papier est analysée la réponse à une représentation simplifiée d'un avion ayant subi deux perturbations quantifiées afin de voir comment la seconde perturbation peut modifier la conduite du système générée par la première.

Le second papier traite d'un modèle mathématique qui peut être utilisé pour le calcul de la réponse dynamique des structures d'un avion opérant sur des surfaces reparées mais rugueuses; la comparaison sera faite entre les prédictions théoriques pour un avion YF16 et les mesures significatives prises à partir d'essais de réponses en mode de fréquence.

CONTENTS

INTERPRETATION IN TERMS OF THE RESPONSE OF A ONE DEGREE-OF-FREEDOM OSCILLATOR TO TWO SUCCESSIVE DISTURBANCES

by

Dr James J.Olsen
Assistant for Research and Technology
Structures and Dynamics Division

Flight Dynamics Laboratory
Air Force Wright Aeronautical Laboratories
Wright-Patterson Air Force Base, Ohio 45433, USA

ABSTRACT

This paper explains the dynamic response of an aircraft that taxies over two arbitrary disturbances, under the assumption that the aircraft can be represented as a linear, one degree-of-freedom system . That analysis produces the concept of the BUMP MULTIPLIER which explicitly and simply determines whether a second discrete disturbance will amplify or attenuate the response from a first disturbance. The BUMP MULTIPLIER also simplifies the understanding and presentation of the results. While the assumptions are very severe, the resulting formulas can be very useful to guide more elaborate nonlinear calculations or to plan test programs.

1. INTRODUCTION

The problem of aircraft dynamic response to taxiing over rough surfaces has been a topic of research for many years. For the most part, the research has been limited to predicting and measuring the dynamic response over the (nearly) random roughness imposed by the terrain or by wear and tear on runways and taxiways. Within the last several years, however, concerns have arisen within the Defense agencies of the NATO countries about the safety of aircraft operations over the discrete disturbances which can arise from bomb-damage to the runways. Those concerns also extend to the dynamic response due to taxi over repaired runways and repetitive aircraft operations on the (potentially) yielding surfaces.

As a result of those concerns the United States Air force instituted program HAVE BOUNCE which is performing taxi tests over simulated (relatively mild) runway damage and repairs for several USAF combat and transport aircraft. the project also develops computer programs to predict the dynamic response to the simulated runway profiles . Other NATO nations are performing similar test and analysis programs on their aircraft.

HAVE BOUNCE considers the computer programs to be *validated* when they produce satisfactory comparisons with the experimental results from flight (taxi) tests. Then the project uses the *validated* computer programs to extrapolate from the relatively mild test conditions to more severe operational cases. Since the computer programs account for the nonlinear properties of the landing gears and tires, the extrapolation of their results beyond their *validated* range of parameters is always open to some question.

Because the taxi test programs have proven to be very expensive, difficult to control and repeat and (sometimes) dangerous, the USAF also created the Aircraft Ground Induced Loads Excitation (AGILE) facility which measures the dynamic response of operational aircraft to damaged and repaired runways within the controlled conditions of the laboratory. The project supports an operational aircraft on its tires on massive hydraulic shakers and drives the shakers vertically to represent the vertical events of the aircraft taxiing over damaged and repaired runways. Each (of the three integrated) shakers can sustain a static weight of 50,000 lb, can displace amplitudes of 10 in, can impose dynamic forces up to 50,000 lb and can be driven sinusoidally (frequencies up to 25 Hz), randomly or to follow prescribed discrete motions. In its first major test, agreement between the AGILE tests and HAVE BOUNCE taxi tests for an operational A-7D aircraft was excellent.

All three evaluation methods computer programs, HAVE BOUNCE taxi tests on operational aircraft and AGILE tests on operational aircraft have been dominated by one major consideration-the nonlinearities in the landing gear. As a result, nearly all of the computations have been done with numerical time-integration of the nonlinear differential equations of motion. The taxi tests and AGILE tests also have been forced to adopt a tedious approach of repetitive, trial and error test cases, again because the aspect of nonlinearity has prevented the superposition of simple disturbances to synthesize more complex responses.

In this paper we contend that the nonlinearities do indeed strongly influence the computational and test results, especially the exact levels of the loads obtained. However, the qualitative response and the selection of speeds, bump heights, and bump spacings which produce large dynamic responses ought to be predictable, for the most part, by simpler linear methods Nonlinear calculations, taxi tests and AGILE tests all ought to be preceded by a substantial amount of linearized calculations which can be done rapidly and can yield much physical insight into those conditions which produce extensive dynamic response. A clever analyst may Bbe able to find the simplicity and intuitive understanding in seemingly complex time histories, which in fact may be not much more than superpositions of many relatively simple events.

The purpose of this paper is to review those linear methods, to show how they yield an understanding of complex time histories and how they can be used to plan nonlinear calculations, taxi tests and AGILE tests. The paper illustrates the principles by treating the response of a linear one degree of freedom oscilllator as it taxies over two successive discrete disturbances, introducing the concept of the BUMP MULTIPLIER.

2. THE RESPONSE OF A ONE DEGREE OF FREEDOM OSCILLATOR TO A SINGLE DISTURBANCE

Assume a one degree of freedom oscillator, with damping less than the critical value, receives some excitation over a period of time, but that the excitation stops at time $t = t_1$.

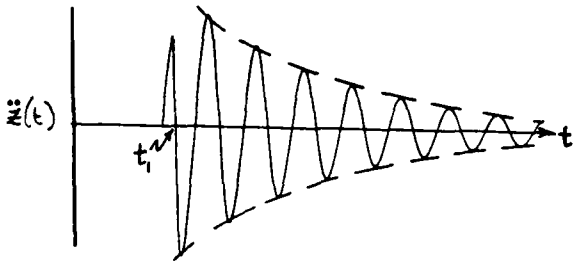

For times after t_1, when the response is decaying freely, the acceleration response can be written:

$$\ddot{z}(t)\Big|_{t>t_1} = e^{-\alpha\omega(t-t_1)}\{A_1 \sin[\omega(t-t_1)] + B_1 \cos[\omega(t-t_1)]\} \tag{2.1}$$

where:

t_1 = the time the excitation ends
ω = damped frequency
$\alpha\omega$ = damping
A_1, B_1 = Constants which depend on α, ω, the excitation and the initial conditions

Note that the damping parameter α above is *not quite the same* as ς, the frequently used fraction of critical damping, which comes from the analysis of a classical one degree-of-freedom oscillator. The product $\alpha\omega$ controls the exponential decay of the damped system, perhaps as observed experimentally. The use of the parameter α allows us to refer the damping to the observed damped frequency ω rather than the fictitious undamped frequency ω_0. In the special case of the classical one degree-of-freedom oscillator $\alpha = \varsigma/\sqrt{1-\varsigma^2}$.

The decaying acceleration response also can be written as:

$$\ddot{z}(t)\Big|_{t>t_1} = R_1 e^{-\alpha\omega(t-t_1)} \sin[\omega(t-t_1) + \phi_1] \tag{2.2}$$

where:

$$R_1 = \sqrt{A_1^2 + B_1^2}$$

$$\tan\phi_1 = B_1/A_1$$

We loosely refer to R_1 as the *potential amplitude* of the acceleration response. It is an upper bound on the amplitude of the acceleration response to a single disturbance. The phase shift ϕ_1 depends only on A_1 and B_1 and will therefore be different for various forms of the excitation.

For small damping ($\alpha << 1$) the behavior of the acceleration response will be dominated by the term $\sin[\omega(t-t_1) + \phi_1]$ in Equation (2.2), so we would expect its local maxima and minima to be obtained from solutions of

$$\omega(t-t_1) + \phi_1 \approx (2n-1)\frac{\pi}{2}; \quad n = 1, 2, 3, \ldots \tag{2.3}$$

However, the term $e^{-\alpha\omega(t-t_1)}$ causes a shift in the values of time for which the local maxima and minima of the acceleration response occur. In fact, the third derivative of the displacement (derivative of the acceleration) is:

$$\frac{d\ddot{z}(t)}{dt}\Big|_{t>t_1} = R_1 e^{-\alpha\omega(t-t_1)}\omega\sqrt{1+\alpha^2}\cos[\omega(t-t_1) + (\phi_1 + \delta_1)] \tag{2.4}$$

where:

$$\tan\delta_1 = \alpha$$

Therefore, the local maxima and minima of the decaying acceleration response will occur at the values of time for which

$$\omega(t-t_1) = (2n-1)\frac{\pi}{2} - (\phi_1 + \delta_1); \quad n = 1, 2, 3, \ldots \tag{2.5}$$

The additional phase shift δ_1 will be small for values of damping that are small with respect to the critical value, ($\alpha << 1$). Note, however, that the first phase shift ϕ_1 need not be small.

We can use these results to obtain an even better upper bound on the amplitude of the acceleration response. If we plug the above value of $\omega(t-t_1)$ into Equation (2.1) for $\ddot{z}(t)_{t>t_1}$, we find that the extreme values for $\ddot{z}(t)_{t>t_1}$ equal:

$$\frac{R_1}{\sqrt{1+\alpha^2}} e^{-\alpha\left[(2n-1)\frac{\pi}{2} - (\phi_1 + \delta_1)\right]}; n = 1, 2, 3, \ldots$$

The largest value occurs for $n = 1$.

3. TWO SUCCESSIVE DISTURBANCES

Now suppose the single degree of freedom oscillator receives a subsequent excitation over another period of time and that excitation stops at time $t = t_2$.

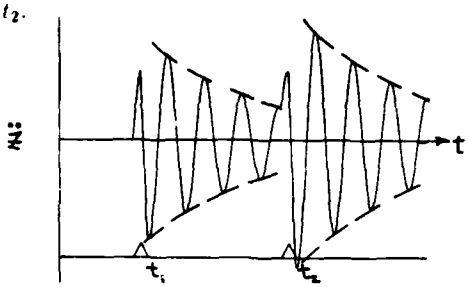

If there had been no previous response from the first disturbance the acceleration response to the second disturbance would have been:

$$\ddot{z}(t)\Big|_{t>t_2} = e^{-\alpha\omega(t-t_2)}\{A_2\sin[\omega(t-t_2)] + B_2\cos[\omega(t-t_2)]\}$$

However, because of the presence of the decaying response to the first disturbance, the acceleration response to the combined disturbances must be written:

$$\begin{aligned}\ddot{z}(t)\Big|_{t>t_2} = {} & e^{\alpha\omega(t-t_1)}\{A_1\sin[\omega(t-t_1)] + B_1\cos[\omega(t-t_1)]\} + \\ & e^{\alpha\omega(t-t_2)}\{A_2\sin[\omega(t-t_2)] + B_2\cos[\omega(t-t_2)]\}\end{aligned} \tag{3.1}$$

For convenience in manipulating the terms in Equation (3.1) we abbreviate:

$$\begin{aligned} e_i &= e^{\alpha\omega(t-t_i)} \\ S_i &= \sin[\omega(t-t_i)] \\ C_i &= \cos[\omega(t-t_i)] \end{aligned}$$

Then the acceleration response to the combined disturbances is:

$$\ddot{z}(t)\Big|_{t>t_2} = e_1(A_1S_1 + B_1C_1) + e_2(A_2S_2 + B_2C_2) \tag{3.2}$$

The trick is write Equations (3.1) and (3.2) with respect to the time of the most recent disturbance, t_2. To that end we write:

$$t - t_1 = (t - t_2) + (t_2 - t_1)$$

We need the additional abbreviations:

$$\begin{aligned} e_{21} &= e^{-\alpha\omega(t_2-t_1)} \\ S_{21} &= \sin[\omega(t_2-t_1)] \\ C_{21} &= \cos[\omega(t_2-t_1)] \end{aligned}$$

To obtain:

$$\begin{aligned} e_1 &= e_2e_{21} \\ S_1 &= S_2C_{21} + C_2S_{21} \\ C_1 &= C_2C_{21} - S_2S_{21} \end{aligned}$$

The acceleration response to the combined excitations becomes

$$\ddot{z}(t)\Big|_{t>t_2} = e_2(A_2^*S_2 + B_2^*C_2) \tag{3.3}$$

where:

$$\begin{aligned} A_2^* &= A_2 + e_{21}(A_1C_{21} - B_1S_{21}) \\ B_2^* &= B_2 + e_{21}(A_1S_{21} + B_1C_{21}) \end{aligned}$$

Following the same procedure we used for the single disturbance, the acceleration response to the combined disturbances can be rewritten as:

$$\ddot{z}(t)\Big|_{t>t_2} = R_2e^{\alpha\omega(t-t_2)}\sin[\omega(t-t_2) + \phi_2] \tag{3.4}$$

where:

$$R_2 = \sqrt{A_2^{*2} + B_2^{*2}} \tag{3.5}$$

$$= \sqrt{(A_2^2 + B_2^2) + 2e_{21}[C_{21}(A_1A_2 + B_1B_2) + S_{21}(A_1B_2 - B_1A_2)] + e_{21}^2(A_1^2 + B_1^2)}$$

$$\tan\phi_2 = \frac{B_2^*}{A_2^*} = \frac{B_2 + e_{21}(A_1S_{21} + B_1C_{21})}{A_2 + e_{21}(A_1C_{21} - B_1S_{21})}$$

Equation (3.5) for R_2, the potential amplitude of the acceleration response to the combined disturbances, is one of the major findings of this paper. Much of the subsequent work here will be concerned with finding the conditions which maximize and minimize R_2.

As we did for the single disturbance, we can differentiate Equation (3.4) with respect to time to search for the times for the local maxima and minima of the acceleration response. We obtain:

$$\frac{d\ddot{z}(t)}{dt}\Big|_{t>t_2} = R_2 e^{-\alpha\omega(t-t_2)}\omega\sqrt{1+\alpha^2}\cos\left[\omega(t-t_2)+(\phi_2+\delta_2)\right] \tag{3.6}$$

where

$$\tan\delta_2 = \alpha$$

We see the same phase shift ($\delta_2 = \delta_1$) in the times for local local maxima and minima of the decaying acceleration response to the combined disturbances, which will occur when

$$\omega(t-t_2) = (2n-1)\frac{\pi}{2} - (\phi_2+\delta_2);\ \ n = 1,2,3,\ldots \tag{3.7}$$

As we did for the single disturbance, we can use these results to obtain an even better upper bound on the amplitude of the acceleration response. If we plug the above value of $\omega(t-t_2)$ into Equation (3.4) for $\ddot{z}(t)_{t>t_2}$, we find that the local extreme values for $\ddot{z}(t)_{t>t_2}$ equal:

$$\frac{R_2}{\sqrt{1+\alpha^2}}e^{-\alpha\left[(2n-1)\frac{\pi}{2}-(\phi_2+\delta_2)\right]};\ n = 1,2,3,\ldots$$

We have seen how to find the times for local maxima and minima of the decaying acceleration response, assuming we know $A_1, B_1, A_2, B_2, \alpha, \omega, t_1$ and t_2. However, we are searching for the best and worst possible runway profiles, so the most critical aspect is to find the values of t_2, the time of the second disturbance, which will locally maximize and minimize the potential amplitude R_2. We differentiate Equation (3.5) for R_2 with respect to t_2 and set the result to zero to obtain:

$$\begin{aligned} &S_{21}\left[(A_1A_2+B_1B_2)+\alpha(A_1B_2-B_1A_2)\right]+\\ &C_{21}\left[\alpha(A_1A_2+B_1B_2)-(A_1B_2-B_1A_2)\right]+\alpha(A_1^2+B_1^2)e_{21}=0 \end{aligned} \tag{3.8}$$

or

$$\dot{R}_{12}\sin\left[\omega(t_2-t_1)+\psi_{12}\right]+\frac{\alpha}{\sqrt{1+\alpha^2}}e^{-\alpha\omega(t_2-t_1)}=0 \tag{3.9}$$

where

$$\dot{R}_{12} = \sqrt{\frac{A_2^2+B_2^2}{A_1^2+B_1^2}}$$

$$\tan\psi_{12} = \frac{\alpha(A_1A_2+B_1B_2)-(A_1B_2-B_1A_2)}{(A_1A_2+B_1B_2)+\alpha(A_1B_2-B_1A_2)}$$

The exact solution for the time delays (t_2-t_1) which locally maximize and minimize R_2 would require a numerical or graphical solution of Equations (3.8) or (3.9), however for small damping we would expect

$$\omega(t_2-t_1) \approx n\pi - \psi_{12};\ \ n = 1,2,3\ldots \tag{3.10}$$

We will give the determination of the time delays (t_2-t_1) an exact treatment in the next Section.

4. THE BUMP MULTIPLIER

Recall that R_1 represented the potential amplitude of the decaying acceleration response to the first disturbance and that R_2 represented the potential amplitude of the acceleration response to the combined disturbances, where in each case we measured time from the time of the most recent disturbance. *We call the ratio R_2/R_1 the BUMP MULTIPLIER, since it defines the extent to which the second disturbance amplifies (or attenuates) the response to the first disturbance.* The BUMP MULTIPLIER is

$$\frac{R_2}{R_1} = \sqrt{\frac{(A_2^2+B_2^2)+2e_{21}\left[C_{21}(A_1A_2+B_1B_2)+S_{21}(A_1B_2-B_1A_2)\right]+e_{21}^2(A_1^2+B_1^2)}{A_1^2+B_1^2}} \tag{4.1}$$

To assist in the interpretation of the BUMP MULTIPLIER we add another set of abbreviations:

$$e_i = \frac{B_i}{A_i};\ i = 1,2$$

The potential amplitudes and phase angles for the responses to the first disturbance and the combined disturbances become:

$$R_1 = |A_1|\sqrt{1+\epsilon_1^2} \tag{4.2}$$

$$\tan\phi_1 = \epsilon_1$$

$$R_2 = |A_2|\sqrt{(1+\epsilon_2^2) + 2\left(\frac{A_1}{A_2}e_{21}\right)[C_{21}(1+\epsilon_1\epsilon_2) + S_{21}(\epsilon_2-\epsilon_1)] + \left(\frac{A_1}{A_2}e_{21}\right)^2(1+\epsilon_1^2)} \tag{4.3}$$

$$\tan\phi_2 = \frac{\epsilon_2 + \left(\frac{A_1}{A_2}e_{21}\right)(S_{21}+\epsilon_1 C_{21})}{1+\left(\frac{A_1}{A_2}e_{21}\right)(C_{21}-\epsilon_1 S_{21})}$$

The BUMP MULTIPLIER becomes:

$$\frac{R_2}{R_1} = \frac{A_2}{|A_1|}\sqrt{\frac{(1+\epsilon_2^2) + 2\left(\frac{A_1}{A_2}e_{21}\right)[C_{21}(1+\epsilon_1\epsilon_2) + S_{21}(\epsilon_2-\epsilon_1)] + \left(\frac{A_1}{A_2}e_{21}\right)^2(1+\epsilon_1^2)}{1+\epsilon_1^2}} \tag{4.4}$$

Note in Equation (4.4) that the magnitude effects are contained mostly in the term $\left|\frac{A_2}{A_1}\right|$, whereas the spacing effects are in the radical. The spacing effects are dominated by the terms

$$S_{21} = \sin[\omega(t_2 - t_1)]$$

$$C_{21} = \cos[\omega(t_2 - t_1)]$$

and those terms are always modulated by the combination

$$\frac{A_1}{A_2}e_{21} = \frac{A_1}{A_2}e^{-\alpha\omega(t_2 - t_1)}$$

When we use these abbreviations in Equation (3.9) to find the time delays $(t_2 - t_1)$ which locally maximize and minimize the potential amplitude R_2, we obtain

$$\left|\frac{A_2}{A_1}\right|\sqrt{\frac{1+\epsilon_2^2}{1+\epsilon_1^2}}\sin[\omega(t_2-t_1)+\psi_{12}] + \frac{\alpha}{\sqrt{1+\alpha^2}}e^{-\alpha\omega(t_2-t_1)} = 0 \tag{4.5}$$

where

$$\tan\psi_{12} = \frac{\alpha(1+\epsilon_1\epsilon_2) - (\epsilon_2-\epsilon_1)}{(1+\epsilon_1\epsilon_2) + \alpha(\epsilon_2-\epsilon_1)}$$

A first approximation for $\alpha << 1$ for the time delays would be:

$$\omega(t_2 - t_1) \approx n\pi - \psi_{12} \quad ; n = 1,2,3,\ldots \tag{4.6}$$

To get a second approximation we search for small angles β_n such that

$$\omega(t_2 - t_1) = n\pi - \psi_{12} - \beta_n \tag{4.7}$$

With this change of variables Equation (4.5) takes a new form

$$C_n \sin\beta_n = \frac{\alpha e^{\alpha\beta_n}}{\sqrt{1+\alpha^2}} \tag{4.8}$$

where

$$C_n = (-1)^n e^{\alpha(n\pi - \psi_{12})}\left|\frac{A_2}{A_1}\right|\sqrt{\frac{1+\epsilon_2^2}{1+\epsilon_1^2}} \tag{4.9}$$

If we expand Equation (4.8) for small β_n, keeping only first order terms, we obtain

$$\beta_n \approx \frac{\alpha}{C_n\sqrt{1+\alpha^2} - \alpha^2} \tag{4.10}$$

This then is the (hoped for) small correction we use in Equation (4.7) to find the second approximation for the time delays $(t_2 - t_1)$.

5. USE OF THE AVERAGE SPEED

We have made no assumption of a constant taxi speed between the two disturbances; in fact we will show in this Section that the spacing effects are dominated by the average speed between them.

If l is the distance between the two disturbances, the average speed is

$$\bar{V} = \frac{l}{t_2 - t_1} \tag{5.1}$$

Then we can express the term

$$\omega(t_2 - t_1) = \frac{l\omega}{\bar{V}} = \bar{\lambda} \tag{5.2}$$

The usual terminology for $\lambda = l\omega/V$, based on the instantaneous speed, is the reduced frequency. Therefore $\bar{\lambda} = l\omega/\bar{V}$ is the reduced frequency based on the average speed between the two disturbances.

Amplitude and Bump Multiplier

Equations (4.2) and (4.3) for the potential amplitudes and phase angles, and Equation (4.4) for the BUMP MULTIPLIER remain unchanged, except that now we note

$$e_{21} = e^{-\alpha\bar{\lambda}}$$

$$S_{21} = \sin\bar{\lambda}$$

$$C_{21} = \cos\bar{\lambda}$$

Best/Worst Runway Profiles

The process for finding the exact and approximate solutions for the time delays which maximize and minimize the potential amplitude R_2 of the decaying acceleration response to the combined disturbances remains unchanged, except Equation (4.5) now becomes:

$$\frac{A_2}{A_1}\sqrt{\frac{1+\epsilon_2^2}{1+\epsilon_1^2}}\sin\left(\bar{\lambda} + \psi_{12}\right) + \frac{\alpha}{\sqrt{1+\alpha^2}}e^{-\alpha\bar{\lambda}} = 0 \tag{5.3}$$

The first approximation for the time delays becomes an equation for $\bar{\lambda}$:

$$\bar{\lambda} \approx n\pi - \psi_{12} \quad ; n = 1, 2, 3, \ldots \tag{5.4}$$

The process of finding exact solutions and second approximations for the time delays also remains unchanged, except that Equation (4.7) becomes

$$\bar{\lambda} = n\pi - \psi_{12} - \beta_n \tag{5.5}$$

6. SPECIAL CASE: SIMILAR DISTURBANCES

We now define similar disturbances as discrete disturbances that have the same shape but differ only in magnitude and/or sign. Examples would be the entire family of infinite ramps or a family of sine waves of the same wavelength but varying heights. *The assumption of similar disturbances is not a very limiting one. In fact, nearly all of the profiles tested in the HAVE BOUNCE program and all of the NATO/AGARD profiles can be broken down into sequences of similar ramp disturbances.* For linear systems with zero initial conditions similar disturbances will produce similar responses, and when disturbances are similar $\epsilon_1 = \epsilon_2 = \epsilon$.

Amplitude

Under the assumption of similar disturbances, Equation (4.2) and (4.3) for the potential amplitudes and phase angles become:

$$R_1 = |A_1|\sqrt{1+\epsilon^2} \tag{6.1}$$

$$\tan\phi_1 = \epsilon$$

$$R_2 = |A_2|\sqrt{1+\epsilon^2}\sqrt{1 + 2\left(\frac{A_1}{A_2}e_{21}\right)C_{21} + \left(\frac{A_1}{A_2}e_{21}\right)^2} \tag{6.2}$$

$$\tan\phi_2 = \frac{\epsilon + \left(\frac{A_1}{A_2}e_{21}\right)(S_{21} + \epsilon C_{21})}{1 + \left(\frac{A_1}{A_2}e_{21}\right)(C_{21} - \epsilon S_{21})}$$

Bump Multiplier

Equation (4.4) for the BUMP MULTIPLIER reduces to:

$$\frac{R_2}{R_1} \quad \frac{A_2}{A_1}\sqrt{1 + 2\left(\frac{A_1}{A_2}e_{21}\right)C_{21} + \left(\frac{A_1}{A_2}e_{21}\right)^2} \tag{6.3}$$

Figures (6.1) and (6.2) illustrate the BUMP MULTIPLIER versus $\bar{\lambda}$ with the damping as a parameter for the special case of equal (or opposite) disturbances at constant speeds.

The major conclusion to be drawn is the dependence of the BUMP MULTIPLIER on the nondimensional spacing (or speed or frequency) parameter

$$\bar{\lambda} = \omega(t_2 - t_1) = l\omega/V$$

The spacing of the disturbances, the average speed of the vehicle and the natural frequency all combine into the one parameter the reduced frequency based on the average speed. Also, while the BUMP MULTIPLIER clearly diminishes with $\bar{\lambda}$ for small values of α, the values of $\bar{\lambda}$ that produce the local minima and maxima are seen to be fairly weak functions of α.

Best/Worst Runway Profiles

In order to find the time delays that locally maximize and minimize the potential amplitude R_2 Equation (5.3) reduces to

$$\frac{A_2}{A_1}\sin\left(\bar{\lambda} + \psi_{12}\right) + \frac{\alpha e^{-\alpha\lambda}}{\sqrt{1+\alpha^2}} = 0 \tag{6.4}$$

where

$$\tan\psi_{12} = \alpha$$

The definition of C_n reduces to:

$$C_n = (-1)^n e^{\alpha(n\pi - \psi_{12})}\frac{A_2}{A_1} \tag{6.5}$$

Tables (6.1) and (6.2) give values of the first approximation, second approximation and exact solution for $\bar{\lambda}$ which locally maximize and minimize the BUMP MULTIPLIER for the same special case of equal (or opposite) disturbances and constant speeds.

The major conclusions to be drawn are:

(a) Again the spacing that maximizes or minimizes the acceleration response depends very weakly on the damping parameter, α.

(b)the First approximation

$$\bar{\lambda} = n\pi - \psi_{12} \approx n\pi - \alpha$$

is an excellent approximation to the exact solution for reasonably small values of damping

7. EXAMPLE: THE CLASSICAL, UNDERDAMPED SPRING MASS DAMPER TAXIING OVER TWO RAMPS.

We consider the example of a classical, single degree of freedom oscillator that encounters two ramp disturbances. The disturbances are separated by a distance l and occur at times t_1 and t_2, respectively. The taxi speeds V_1, V_2 are not necessarily equal at the time of the encounters, nor are the ramp angles θ_1, θ_2.

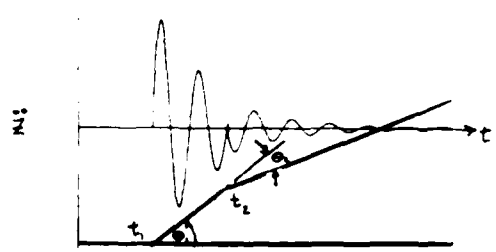

The differential equation of motion is:

$$m\ddot{z} + c\dot{z} + kz = c\dot{g} + kg \tag{7.1}$$

where

$$g(t) = V\theta t\, u(t)$$

$u(t)$ = unit step function

By solving the ordinary differential equation of motion for the displacement in response to the ramp inputs (with zero initial conditions) and then differentiating those results twice with respect to time we find the various parameters to use in Equations (2.1) and (3.1):

$$\begin{aligned} A_i &= V_i\omega_0\theta_i\,(1-2\zeta^2) \\ B_i &= 2V_i\omega_0\theta_i\,\zeta\sqrt{1-\zeta^2} \\ \zeta &= \text{ratio of damping to critical value, } c/2m\omega_0 \\ \omega_0 &= \text{undamped natural frequency, } \sqrt{k/m} \\ \omega &= \text{damped frequency, } \omega_0\sqrt{1-\zeta^2} \\ \alpha &= \zeta/\sqrt{1-\zeta^2} \end{aligned} \tag{7.2}$$

We also note the nondimensional reduced frequencies :

$$\lambda_0 = \frac{l\omega_0}{V}$$

$$\lambda = \frac{l\omega}{V} = \lambda_0\sqrt{1-\zeta^2} \tag{7.3}$$

and the relationship:

$$\alpha\omega = \zeta\omega_0 \tag{7.4}$$

Note the distinction between the hypothetical undamped frequency ω_0 and the actual damped frequency ω. Note also the distinction between ζ, the fraction of critical damping as related to the hypothetical undamped frequency ω_0, and α which we use to relate damping to the actual damped frequency ω.

For purposes of illustration we pick the fictitious undamped natural frequency to be

$$\omega_0 = 2\pi\ rad/sec$$

$$f_0 = \omega_0/2\pi = 1.0\,Hz,$$

and we pick the damping value

$$\zeta = c/2m\omega_0 = 0.1$$

so that

$$\sqrt{1-\zeta^2} = 0.9950$$

$$\alpha = \zeta/\sqrt{1-\zeta^2} = 0.1005$$

Note that this means the actual damped frequency is:

$$\omega = 1.99\pi\ rad/sec;\ f = 0.9950\,Hz$$

All members of the family of ramp inputs are similar. Therefore, For every ramp input (regardless of speed V, frequency ω or slope θ) the similarity parameter ϵ is:

$$\epsilon_1 = \epsilon_2 = \epsilon = \frac{B}{A} = \frac{2\zeta\sqrt{1-\zeta^2}}{1-2\zeta^2} = \tan\phi_1 = 0.2030 \tag{7.5}$$

The second phase shifts for the location of the local maxima and minima of the decaying acceleration response will be identical:

$$\delta_1 = \delta_2 = \delta = \sin^{-1}\zeta = 0.1002\,rad = 5.739^\circ$$

Figure (7.1) illustrates the two phase shifts ϕ_1 and δ versus the damping ratio ζ.

Amplitude

The potential amplitudes of the decaying acceleration responses are obtained by applying the definitions in equations (7.2) (7.4) to the equations for similar disturbances, Equations (6.1) (6.5).

Figure (7.2) illustrates the decaying acceleration response of the classical spring mass damper for a typical single ramp input at a constant speed of $V = 10.0\ l/sec$, where the length units are in any convenient, consistent system. Figure (7.3) illustrates the sensitivity to speed by plotting the response for a range of speeds $V = 10, 11, \ldots, 20\ l/sec$. Note that the amplitude of the response to the single disturbance grows monotonically with increasing speed. Figure (7.4) illustrates a curious feature in the dependence of the response on damping for

$$\zeta = 0.1, 0.2, \ldots, 0.5$$

at a constant speed of $V = 10.0\ l/sec$. Large values of damping actually increase the peak acceleration response at the earliest instants of time. These effects are the result of the term

$$B_i = 2V_i\omega_0\theta_i\,\zeta\sqrt{1-\zeta^2}$$

which reaches its maximum value at $\zeta = \frac{1}{2}^2$

Figure (7.5) illustrates the decaying acceleration response for traversing two equal (but opposite) ramps, separated by a distance of 20.0 l,at a constant speed of 10.0 l/sec. Note that the maximum amplitude of the acceleration response to the combined disturbances at a speed of 10.0 l/sec is actually smaller than the response to the first disturbance alone at the same speed. Figures (7.6) and (7.7) show that this will not always be the case. By changing the constant speeds to V = 8.02 and 13.46 l/sec for the same ramp geometry, we see that the response to the combined disturbances can be markedly greater than the response to the first disturbance alone. Figure (7.8) further illustrates the sensitivity to speed by plotting the response for a range of speeds $V = 10, 11, \ldots, 20\ l/sec$. While the amplitude of the response to the single disturbance grew monotonically with increasing speed, the amplitude of the response to the combined disturbances displays a much more complicated structure.

Figure (7.9) shows the damping effect on the acceleration response to the combined disturbances. Note how the maximums, zeroes and minimums occur at nearly the same periodic values of $\tilde{\lambda}$, regardless of the value of the critical damping ratio ζ.

Bump Multiplier

Reverting to the general case of non-constant speeds and ramp angles, the potential amplitude for the dynamic acceleration response to the combined disturbances is given by:

$$R_2 = V_2 \omega_0 |\theta_{21}| \sqrt{1 + 2\left(\frac{V_1\theta_1 e_{21}}{V_2\theta_2}\right) e_{21} C_{21} + \left(\frac{V_1\theta_1 e_{21}}{V_2\theta_2}\right)^2} \tag{7.6}$$

where:

$$e_{21} = e^{-\alpha(t_2 - t_1)} = e^{-\alpha\tilde{\lambda}} = e^{-0.1005\tilde{\lambda}}$$

$$C_{21} = \cos[\omega(t_2 - t_1)] = \cos\tilde{\lambda}$$

The BUMP MULTIPLIER from Equation (6.3) is

$$\frac{R_2}{R_1} = \frac{V_2\theta_2}{V_1\theta_1} \sqrt{1 + 2\left(\frac{V_1\theta_1 e_{21}}{V_2\theta_2}\right) C_{21} + \left(\frac{V_1\theta_1 e_{21}}{V_2\theta_2}\right)^2} \tag{7.7}$$

The term $\frac{1}{2}\frac{\theta_2}{\theta_1}$ in Equation (7.7) gives the pure magnitude effect of the two disturbances. The radical gives the spacing effect. The dominant term is $C_{21} = \cos\tilde{\lambda}$, which is modified by

$$\left(\frac{V_1\theta_1}{V_2\theta_2}\right) e_{21} = \left(\frac{V_1\theta_1}{V_2\theta_2}\right) e^{-\alpha\tilde{\lambda}} = \left(\frac{V_1\theta_1}{V_2\theta_2}\right) e^{-0.1005\tilde{\lambda}}$$

Equations (7.6) and (7.7) are **very powerful results** *which relate the potential amplitude R_2 and the BUMP MULTIPLIER to the instantaneous speeds V_1, V_2, the average speed $\bar{V}$, the ramp angles θ_1, θ_2, the damping parameter α and the average reduced frequency $\tilde{\lambda} = l\omega/\bar{V}$*

Best/Worst Runway Profiles

Recall that the equations which determine the best/worst runway profiles or speeds were:

$$\frac{A_2}{A_1}\sin(\tilde{\lambda} + \psi_{12}) + \frac{\alpha e^{-\alpha\tilde{\lambda}}}{\sqrt{1+\alpha^2}} = 0 \tag{6.4}$$

where

$$\tan\psi_{12} = \alpha$$

For this example

$$\psi_{12} = \sin^{-1}\zeta = 0.1002\ rad = 5.739°$$

For constant speeds and equal (but opposite) ramps Equation (6.4) reduces to

$$e^{-\tilde{\lambda}} + \sin(\tilde{\lambda} + \psi_{12}) = 0 \tag{7.8}$$

a. First Approximation

The first approximation to the time delays that locally maximize and minimize the acceleration response to the combined disturbances is:

$$\lambda \approx n\pi - \psi_{12}; \quad n = 1, 2, 3 \ldots \tag{5.4}$$

or

$$\lambda = 3.0414, 6.1830, 9.3246, 12.4662, \ldots$$

b. Exact Solution

In obtaining the exact solution for the time delays, the values of C_n for $n = 1, 2, 3 \ldots$ are:

$$C_n = 21.04; \; -486.9; \; 11270; \; -310,700 \ldots$$

The corresponding exact (rapidly diminishing) values of λ_n are:

$$\lambda_n = 4.779 \cdot 10^{-3}, \quad 2.064 \cdot 10^{-4}, 8.920 \cdot 10^{-6}, \; -3.855 \cdot 10^{-7} \ldots$$

and the exact values of λ are:

$$\lambda = 3.0366, 6.1832, 9.3246, 12.4662, \ldots$$

These small values of λ_n illustrate why the first approximation is such an excellent approximation.

c. Second Approximation

The approximate solutions for small α would be

$$\lambda_n \approx \frac{\alpha}{C_n\sqrt{1+\alpha^2} - \alpha^2} \tag{4.10}$$

These approximations to λ_n are

$$\lambda_n = 4.774 \cdot 10^{-3}; \; -2.064 \cdot 10^{-4}, \ldots$$

They differ from the exact values only for $n = 1$, and then very slightly. In addition, both the exact solutions and the second approximations are very small corrections to the first approximation:

$$\lambda = n\pi - \psi_{12} \approx n\pi - \alpha \tag{5.4}$$

Earlier in this section, when we found the speeds $8.02 \, and \, 13.46 \, l/sec$ that increased the response to two equal (but opposite) disturbances separated by a distance $20.0 \, l$, we used the results in Table (7.2). Table (7.2) shows that, for $\alpha \approx 0.1$, the exact solutions for the values of the reduced frequency $\tilde{\lambda} = l\omega/\tilde{V}$ that maximize and minimize the acceleration response to the combined disturbances are:

Maximize: $\tilde{\lambda}/\pi = 0.9447, 2.9558, 4.9616, \ldots$
Minimize: $\tilde{\lambda}/\pi = 1.9853, 3.9774, 5.9731, \ldots$

For a length $l = 20.0 \, l$, and noting that $f = \omega/2\pi = 0.995 \, Hz$, these results translate to the following speeds:

Maximize: $V = 42.13, 13.46, 8.02 \, l/sec, \ldots$
Minimize: $V = 20.05, 10.01, 6.66 \, l/sec, \ldots$

Note that Table (7.1) or (7.2) requires the use of the damped reduced frequency, $\tilde{\lambda} = l\omega/\tilde{V}$ rather than the the fictitious undamped reduced frequency $\tilde{\lambda}_0 = l\omega_0/\tilde{V}$.

8. APPLICATION TO NONLINEAR CALCULATIONS AND TEST PROGRAMS

a. Three Principles

The first set of basic ideas to keep in mind when when using these results to plan nonlinear calculations, HAVE BOUNCE (taxi) tests or AGILE tests is that a useful building block is the *infinite ramp*, that two infinite (opposite) ramps can combine to produce an *AGARD Bump*, and that two (opposite) AGARD bumps can combine to produce an *AGARD Repair Mat*.

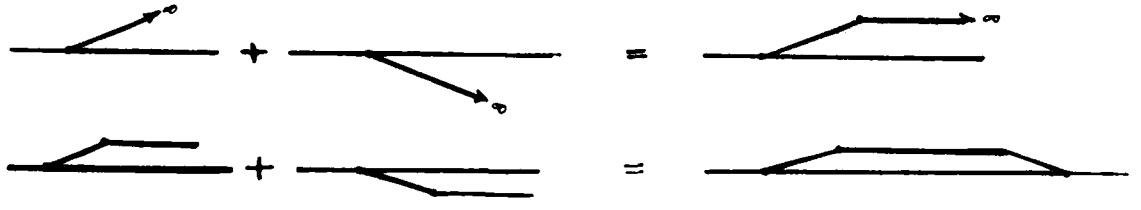

Second, recall that for two disturbances separated by a distance l, the best/worst combinations tend to occur when:

$$\tilde{\lambda} = \frac{l\omega}{\tilde{V}} = \frac{2\pi l f}{\tilde{V}} \approx n\pi - \alpha \; ; n = 1, 2, 3 \ldots$$

or

$$\tilde{V} \approx \frac{2lf}{n - \frac{\alpha}{\pi}}) \; ; n = 1, 2, 3 \ldots \tag{8.1}$$

Third, the *potential amplitudes* of the acceleration response of a classical one degree-of-freedom oscillator to a single infinite ramp and to two combined ramps are:

$$R_1 = V_1\omega_0|\theta_1|$$

$$R_2 = \omega_0\sqrt{(V_2\theta_2)^2 + 2(V_1\theta_1)(V_2\theta_2)e_{21}C_{21} + (V_1\theta_1)^2}$$

$$= V_2\omega_0|\theta_2|\sqrt{1 + 2\left(\frac{V_1\theta_1 e_{21}}{V_2\theta_2}\right)C_{21} + \left(\frac{V_1\theta_1 e_{21}}{V_2\theta_2}\right)^2} \tag{7.6}$$

where:

$$e_{21} = e^{-\alpha\omega(t_2 - t_1)} = e^{-\alpha\tilde{\lambda}}$$

$$C_{21} = \cos[\omega(t_2 - t_1)] = \cos\tilde{\lambda}$$

b. The Response on the Initial Slope of a Repair Mat

Beginning with the basic building block of the *infinite ramp* we have shown that the acceleration response is given by:

$$\ddot{z}(t)\big|_{t>t_1} = R_1 e^{-\alpha\omega(t-t_1)}\sin[\omega(t - t_1) + \phi_1] \tag{2.2}$$

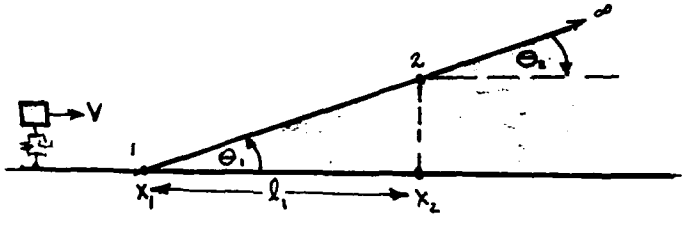

The initial acceleration response at the first corner will be given by:

$$\ddot{z}\big|_{t=t_1^+} = R_1\sin\phi_1 \tag{8.2}$$

We have also shown that the local extreme values of the acceleration response are given by:

$$\frac{R_1}{\sqrt{1+\alpha^2}}e^{-\alpha\left[(2n-1)\frac{\pi}{2} - (\phi_1 + \delta_1)\right]} \; ; n = 1, 2, 3, \ldots$$

and that the peak values occur when

$$\omega(t_{peak} - t_1) = (2n-1)\frac{\pi}{2} - (\phi_1 + \delta_1) \; ; n = 1, 2, 3, \ldots$$

This translates to distances where the peaks occur of:

$$x_{peak} - x_1 = \frac{\tilde{V}}{\omega}\left[(2n-1)\frac{\pi}{2} - (\phi_1 + \delta_1)\right] \; ; n = 1, 2, 3, \ldots$$

or

$$x_{peak} - x_1 = \frac{(2n-1)\tilde{V}}{4f}\left[1 - \frac{2(\phi_1 + \delta_1)}{\pi(2n-1)}\right] \; ; n = 1, 2, 3, \ldots \tag{8.3}$$

where $\tilde{V}$ is the average speed over the initial slope.

These are the expressions for the peak amplitudes of the acceleration response and the locations of those peak responses on the initial slope of an ***AGARD Repair Mat.*** Conversely, if the length of the initial ramp is l_1, we know that the peaks of the acceleration response will occur somewhere on the ramp for speeds:

$$\tilde{V} \leq \frac{4fl_1}{(2n-1)\left[1 - \frac{2(\phi_1 + \delta_1)}{\pi(2n-1)}\right]} \; ; n = 1, 2, 3, \ldots \tag{8.4}$$

Otherwise the peak acceleration responses on the initial slope will occur at the second corner. At that point the value becomes:

$$\ddot{z}\big|_{t\ t_2} = R_1 e^{-\alpha\left(\frac{l_1\omega}{V}\right)}\sin\left(\frac{l_1\omega}{V} + \phi_1\right) \tag{8.5}$$

c. The Flat Area of a Repair Mat

We assume that angles θ_1, θ_2 are equal and opposite and that l_1, the length of the ramp, is small enough so that the speed over the initial slope is constant, $V_1 = V_2$. Then the acceleration response to the combined disturbances is:

$$\ddot{z}(t)\big|_{t>t_2} = R_2 e^{-\alpha\omega(t-t_2)} \sin[\omega(t-t_2)+\phi_2] \tag{3.4}$$

where

$$R_2 = V_1\omega_0|\theta_1|\sqrt{1-2e_{21}C_{21}+e_{21}^2}$$

$$\tan\phi_2 = \frac{\epsilon - e_{21}(S_{21}+\epsilon C_{21})}{1-e_{21}(C_{21}-\epsilon S_{21})}$$

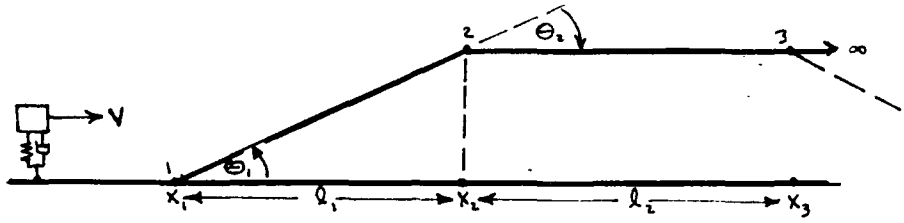

The acceleration response just after the second corner is:

$$\ddot{z}_2\big|_{t=t_2^+} = R_2 \sin\phi_2 \tag{8.6}$$

The local peak values of the acceleration response on the flat part of the repair mat are given by:

$$\frac{R_2}{\sqrt{1+\alpha^2}} e^{-\alpha\left[\frac{(2n-1)\pi}{2} - (\phi_2+\delta_2)\right]} \; ; n = 1,2,3,\ldots$$

and the peak values occur when

$$(2n-1)\pi$$

This translates to distances where the peaks occur of:

$$x_{peak} - x_2 = \frac{\tilde{V}}{\omega}\left[\frac{(2n-1)\pi}{2} - (\phi_2+\delta_2)\right] \; ; n = 1,2,3,\ldots$$

or

$$x_{peak} - x_2 = \frac{(2n-1)\tilde{V}}{4f}\left[1 - \frac{2(\phi_2+\delta_2)}{\pi(2n-1)}\right] \; ; n = 1,2,3,\ldots \tag{8.7}$$

where in this case $\tilde{V}$ is the average speed over the flat part of the repair mat. If the length of the flat part is l_2, we know that peak acceleration responses will occur somewhere on the flat part for speeds:

$$\tilde{V} \le \frac{4fl_2}{(2n-1)\left[1 - \frac{2(\phi_2+\delta_2)}{\pi(2n-1)}\right]} \; ; n = 1,2,3,\ldots \tag{8.8}$$

d. Obtaining the Infinite Ramp Data from the Test Results for an AGARD BUMP

Because of the impossibility of experimentally developing an *Infinite Ramp*, it will be more practical to excite the oscillator with an *AGARD Bump* and then infer what the response would be to an *Infinite Ramp*. We assume that we have excited the oscillator with an *AGARD Bump* and, therefore, we will know e_{21}, S_{21} *and* C_{21} and will have measured $R_2, \alpha, \omega, \phi_2$ in the equation:

$$\ddot{z}(t)\big|_{t>t_2} = R_2 e^{-\alpha\omega(t-t_2)} \sin[\omega(t-t_2)+\phi_2] \tag{3.4}$$

The potential amplitude R_1 can be obtained from:

$$R_1 = \frac{R_2}{\sqrt{1-2e_{21}C_{21}+e_{21}^2}} \tag{8.9}$$

Then the phase lag ϕ_1 can be obtained from:

$$Q = \frac{e_{21}S_{21}}{1-e_{21}C_{21}} \tag{8.10}$$

$$\epsilon = \frac{\tan\phi_2 + Q}{1 - Q\tan\phi_2} \tag{8.11}$$

$$\tan\phi_1 = \epsilon$$

e. Guidelines for Nonlinear Calculations, AGILE Tests and Taxi Tests We begin by calculating or measuring the acceleration response to an *AGARD Bump*

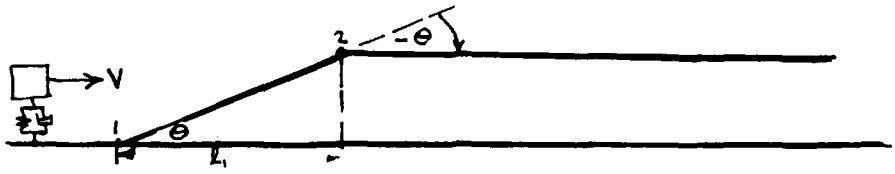

over a range of speeds V and angles θ. Since the response will undoubtedly not be purely in a single degree of freedom, we must process the test data to obtain separate values of R_2, α, ω *and* ϕ_2 for *each degree of freedom*. Then for each speed, angle and degree of freedom we calculate:

$$e_{21} = e^{-\alpha\omega(t_2 - t_1)};\ C_{21} = \cos[\omega(t_2 - t_1)]$$

and we use Equations (8.9) (8.11) to calculate R_1 *and* ϕ_1. A good test of our assumed linearity is to form $\frac{R_1}{(V\theta)}$. The values should be approximately the same for each degree of freedom, regardless of speed V or angle θ.

The next step should be to test the linear result that the Best/Worst *AGARD Bumps* will be those for which

$$\lambda = \frac{l_1\omega}{V} = n\pi - \alpha\ ;\ n = 1, 2, 3 \ldots$$

Since l_1 is fixed by the AGARD geometry, we can accomplish this variation by choosing the speeds to be

$$V = \frac{l_1\omega}{n\pi - \alpha}$$

We can interpret the final slope of the *AGARD Repair Mat*

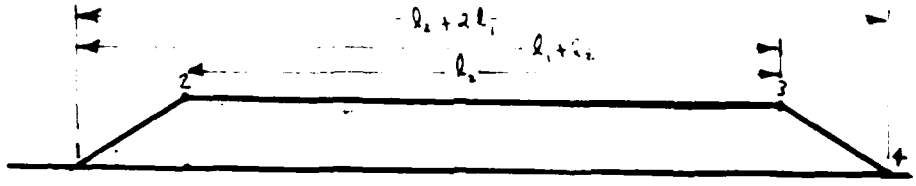

as just the negative of the initial slope; with the only distinction that it occurs at a distance of $l_1 + l_2$ after the initial slope. Then we can search for the Best/Worst length of the repair mat by setting

$$\lambda = \frac{(l_1 + l_2)\omega}{V} = n\pi - \alpha;\ n = 1, 2, 3 \ldots$$

In this case we have both the average speed V and the length l_2 to use as variables.

Now we note that the total length of the *AGARD Repair Mat* is $2l_1 + l_2$ and assume that another repair mat is placed a distance l_3 behind the first mat.

Therefore, to look for the Best/Worst spacings we set

$$\lambda = \frac{(2l_1 + l_2 + l_3)\omega}{V} = n\pi - \alpha;\ n = 1, 2, 3 \ldots$$

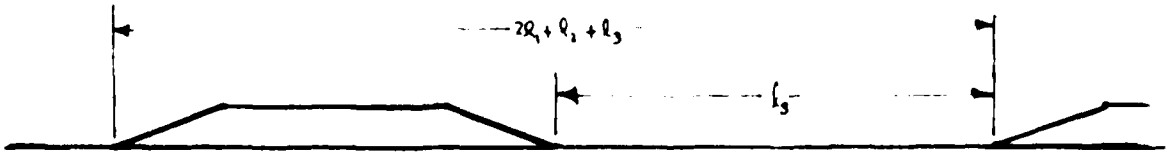

9. CONCLUSIONS

We have treated the dynamic response of an aircraft taxiing over runway disturbances, under the assumption that the gross aspects of the dynamic response can be found in the analysis of a linear, one degree of freedom system, excited by two successive disturbances. We have found:

a. There is a great deal that can be learned about the governing physics for aircraft dynamic response to taxi over damaged and repaired runways by examining the results of calculations with relatively simple, linear models.

b. The seemingly complicated time histories can be merely superpositions of relatively simple, time-phased events.

c. Relatively simple expressions are available for the potential amplitude (an upper bound) of the acceleration response excited by one or two disturbances. In the (not too) special case of *similar*, disturbances separated by a distance l, with nonconstant speeds and ramp angles, the expression for the potential amplitude R_2 is:

$$R_2 = V_2 \omega_0 |\theta_2| \sqrt{1 + 2\left(\frac{V_1\theta_1 e_{21}}{V_2\theta_2}\right) C_{21} + \left(\frac{V_1\theta_1 e_{21}}{V_2\theta_2}\right)^2}$$

where

$$e_{21} = e^{-\alpha\hat{\lambda}}$$
$$C_{21} = \cos\hat{\lambda}$$
$$\hat{\lambda} = l\omega/\bar{V}$$

d. The effects of disturbance spacing and variable taxi speed are controlled by the reduced frequency, based on the average speed between disturbances.

e. One need not actually calculate the time histories to find the best/worst profiles and speeds, but can use the expressions for the potential amplitude R_2 and the BUMP MULTIPLIER $\frac{R_2}{R_1}$.

f. To maximize/minimize dynamic response a good approximation for $\hat{\lambda}$ is

$$\hat{\lambda} = n\pi - \alpha$$

g. While damping obviously controls the dynamic response to the disturbances, the critical speeds and disturbance spacings are weak functions of damping.

h. These results can easily be extended from two disturbances to an arbitrary number of disturbances and multiple degree of freedom systems with multiple landing gear.

i. The results of calculations based on these linear methods should be compared with results from flight(taxi) tests, AGILE tests and nonlinear calculations. This is not to say that the linear results should be relied on to predict detailed loads; rather the question should be *do the simple linear models predict the critical speeds and spacings so that we can use them to guide our test programs and nonlinear solutions.*

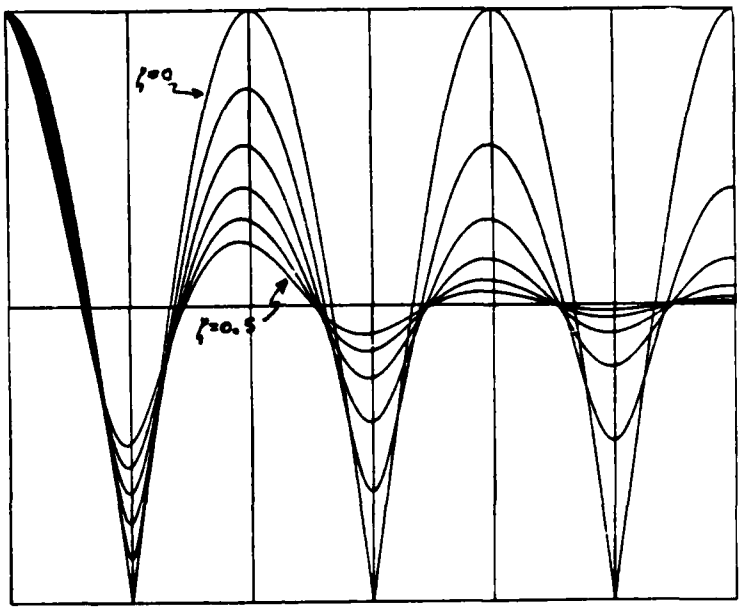

(b) $\zeta = 0, 0.05, 0.10, \ldots, 0.25$

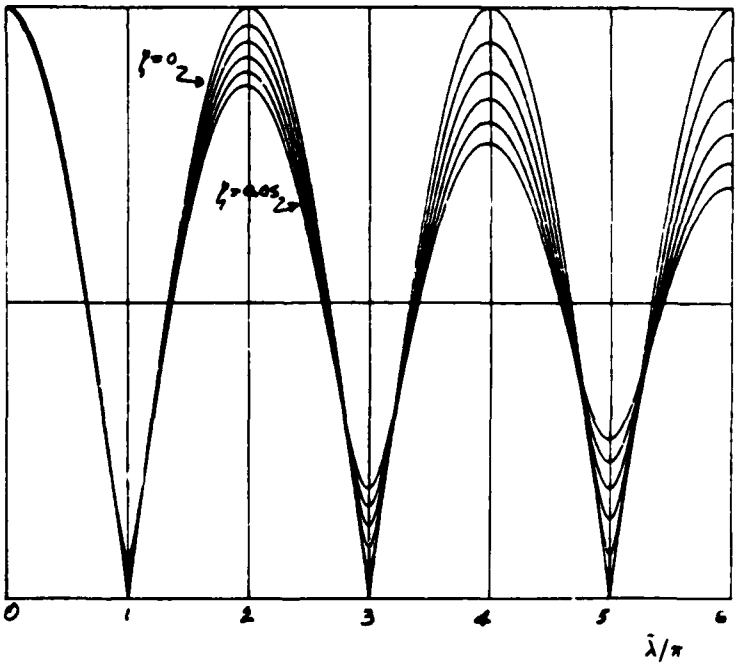

(a) $\zeta = 0, 0.01, 0.02, \ldots, 0.05$

Figure 6.1 The BUMP MULTIPLIER for Equal Disturbances

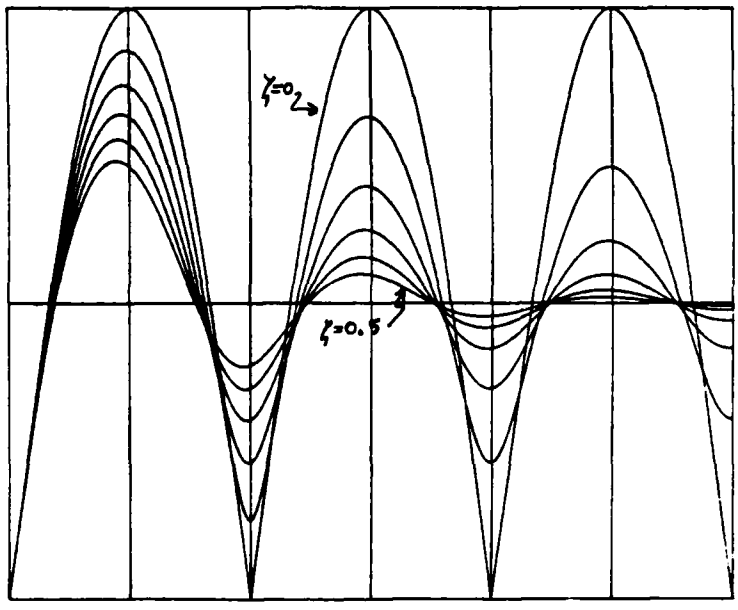

(b) $\varsigma = 0, 0.05, 0.10, \ldots, 0.25$

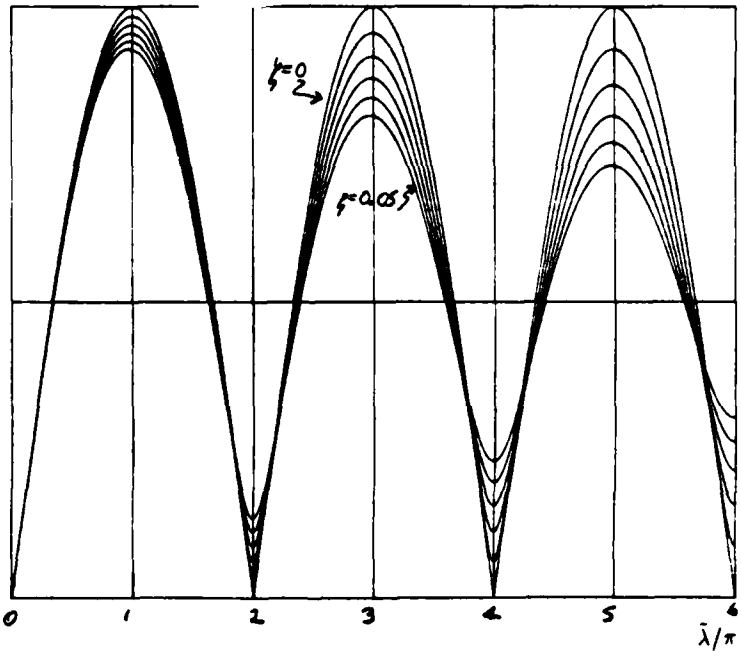

(a) $\varsigma = 0, 0.01, 0.02, \ldots, 0.05$

Figure 6.2 The BUMP MULTIPLIER fot Equal and Opposite Disturbances

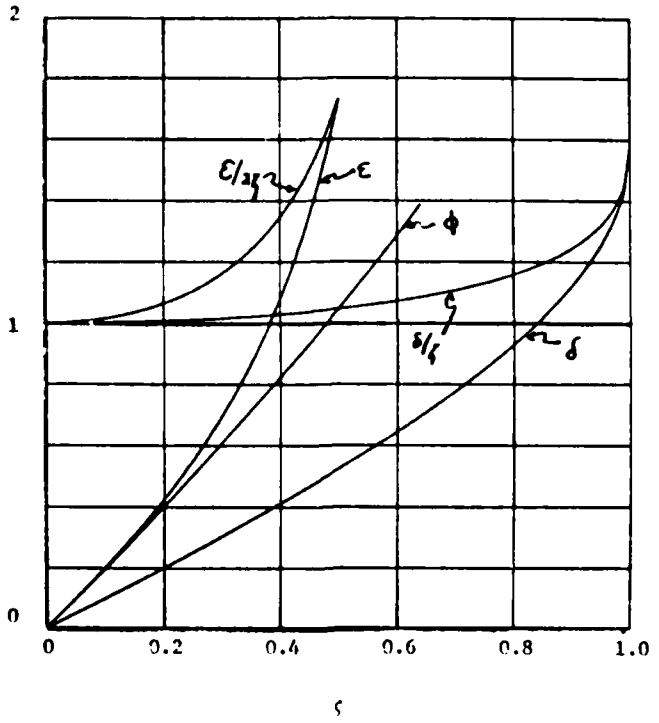

Figure 7.1 The Similarity parameter ϵ and the Phase Angles ϕ and δ

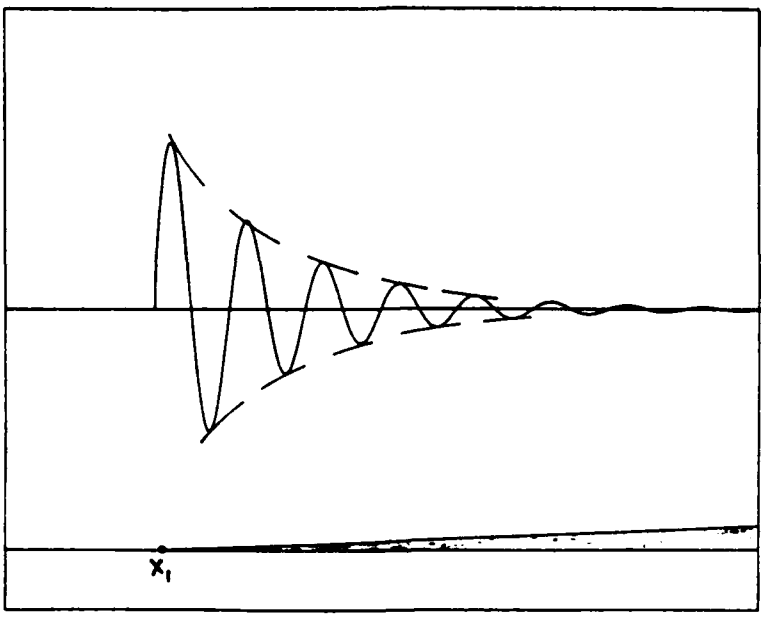

Figure 7.2 Acceleration Response to a Single Ramp at $V = 10.0 l/sec$

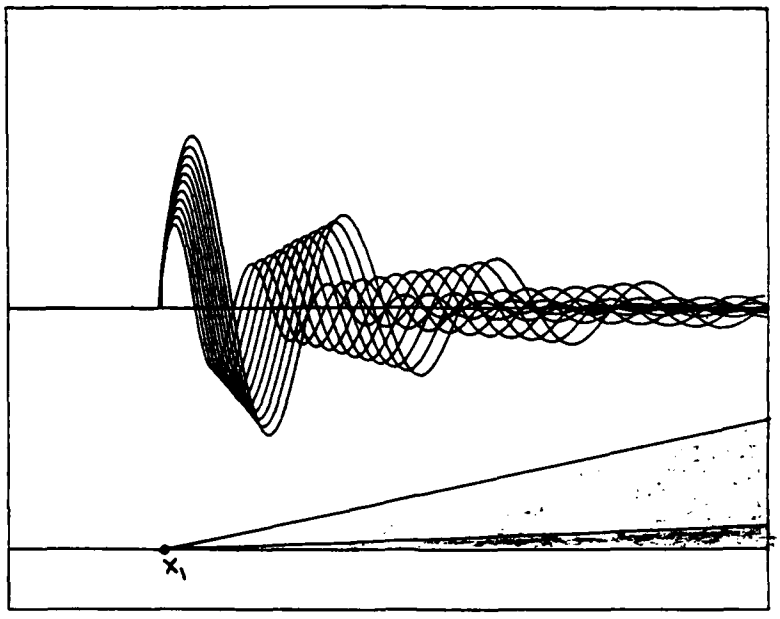

Figure 73 Acceleration Response to a Single Ramp at $V = 10, 11, \ldots, 20 l/sec$

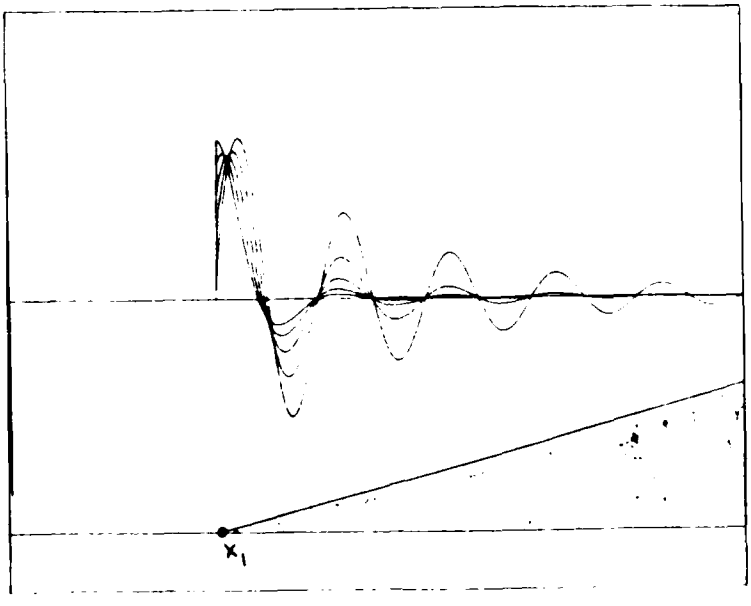

Figure 74 Acceleration Response to a Single Ramp for $\varsigma = 0.1, 0.2, \ldots, 0.5$

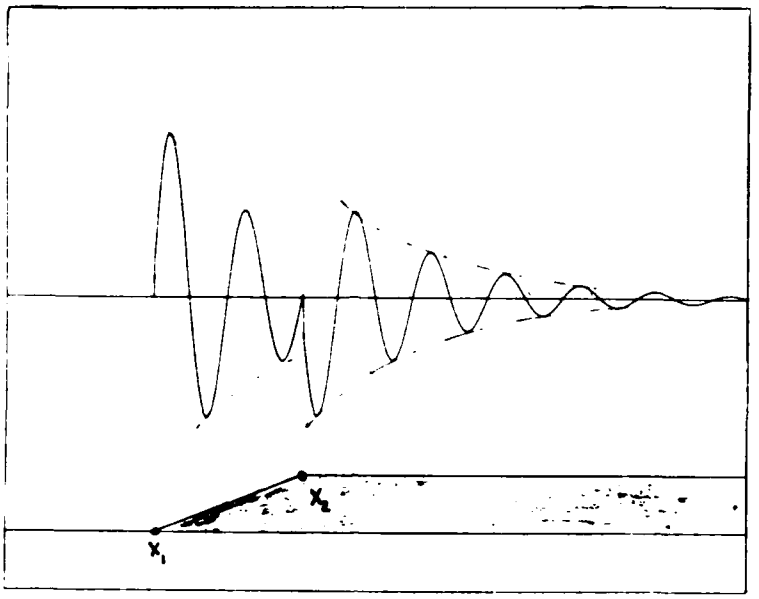

Figure 7.5 Acceleration Response to Two Equal and Opposite Ramps at $V = 10.0 l/sec$

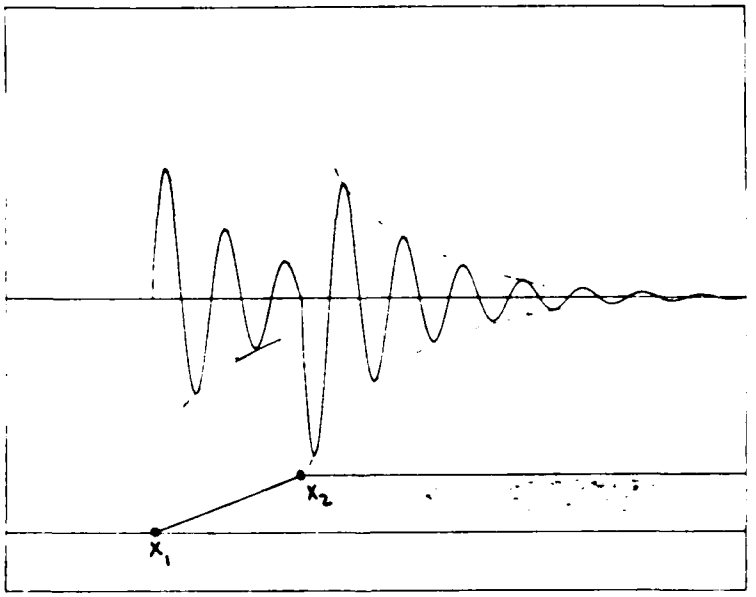

Figure 7.6 Acceleration Response to Two Equal and Opposite Ramps at $V = 8.02 l/sec$

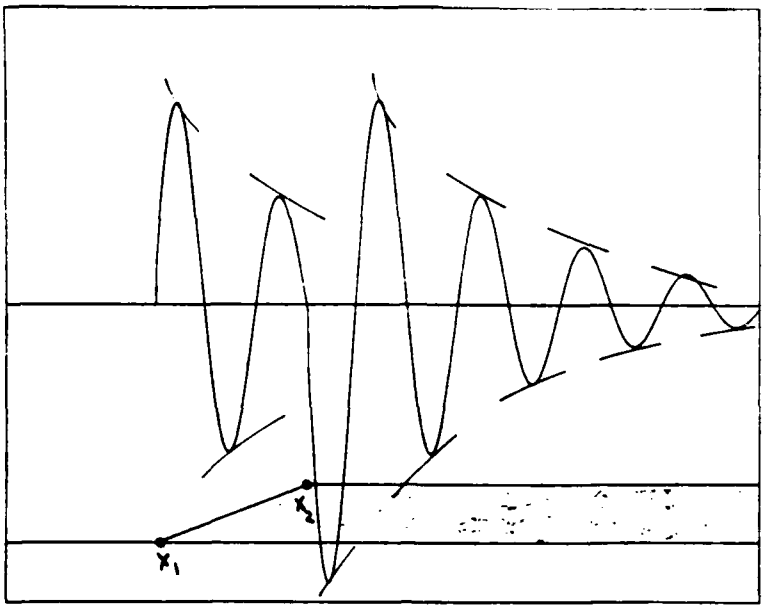

Figure 7.7 Acceleration Response to Two Equal and Opposite Ramps at $V = 13.46 l/sec$

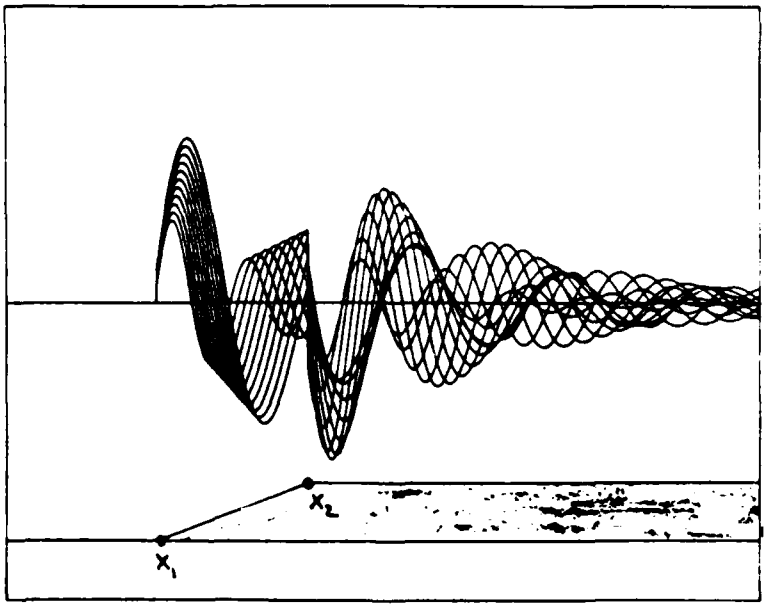

Figure 7.8 Acceleration Response to Two Equal and Opposite Ramps at $V = 10, 11, \ldots, 20 l/sec$

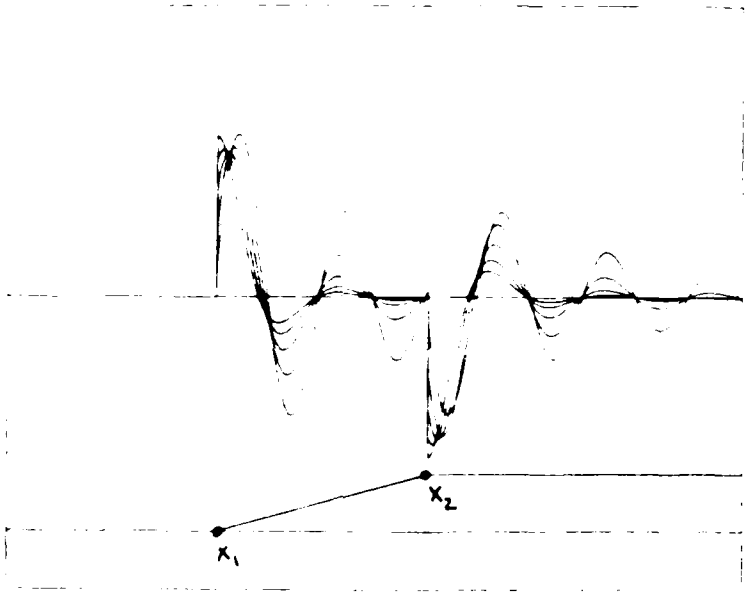

Figure 7.9 Acceleration Response to Two Equal and Opposite Ramps for $\zeta = 0.1, 0.2, \ldots, 0.5$

	n	1st	2nd	Exact
0.0000				
	1	1.0000	1.0000	1.0000
	2	2.0000	2.0000	2.0000
	3	3.0000	3.0000	3.0000
	4	4.0000	4.0000	4.0000
	5	5.0000	5.0000	5.0000
	6	6.0000	6.0000	6.0000
0.0100				
	1	0.9968	0.9937	0.9999
	2	1.9968	1.9938	1.9998
	3	2.9968	2.9939	2.9997
	4	3.9968	3.9940	3.9940
	5	4.9968	4.9941	4.9995
	6	5.9968	5.9942	5.9942
0.0200				
	1	0.9936	0.9877	0.9996
	2	1.9936	1.9880	1.9880
	3	2.9936	2.9884	2.9989
	4	3.9936	3.9887	3.9887
	5	4.9936	4.9890	4.9983
	6	5.9936	5.9893	5.9893
0.0300				
	1	0.9905	0.9818	0.9991
	2	1.9905	1.9825	1.9825
	3	2.9905	2.9832	2.9977
	4	3.9905	3.9839	3.9839
	5	4.9905	4.9845	4.9964
	6	5.9905	5.9850	5.9850
0.0400				
	1	0.9873	0.9760	0.9985
	2	1.9873	1.9774	1.9773
	3	2.9873	2.9785	2.9960
	4	3.9873	3.9796	3.9796
	5	4.9873	4.9805	4.9541
	6	5.9873	5.9813	5.9813
0.0500				
	1	0.9841	0.9704	0.9977
	2	1.9841	1.9724	1.9724
	3	2.9841	2.9741	2.9940
	4	3.9841	3.9756	3.9756
	5	4.9841	4.9768	4.9914
	6	5.9841	5.9779	5.9779

	n	1st	2nd	Exact
0.0000				
	1	1.0000	1.0000	1.0000
	2	2.0000	2.0000	2.0000
	3	3.0000	3.0000	3.0000
	4	4.0000	4.0000	4.0000
	5	5.0000	5.0000	5.0000
	6	6.0000	6.0000	6.0000
0.0500				
	1	0.9841	0.9704	0.9977
	2	1.9841	1.9724	1.9724
	3	2.9841	2.9741	2.9940
	4	3.9841	3.9756	3.9756
	5	4.9841	4.9768	4.9914
	6	5.9841	5.9779	5.9779
0.1000				
	1	0.9683	0.9447	0.9915
	2	1.9683	1.9511	1.9511
	3	2.9683	2.9558	2.9807
	4	3.9683	3.9591	3.9591
	5	4.9683	4.9616	4.9749
	6	5.9683	5.9634	5.9634
0.1500				
	1	0.9526	0.9220	0.9824
	2	1.9526	1.9336	1.9336
	3	2.9526	2.9408	2.9643
	4	3.9526	3.9453	3.9452
	5	4.9526	4.9480	4.9572
	6	5.9526	5.9497	5.9497
0.2000				
	1	0.9372	0.9018	0.9712
	2	1.9372	1.9185	1.9185
	3	2.9372	2.9272	2.9478
	4	3.9372	3.9319	3.9319
	5	4.9372	4.9344	4.9400
	6	5.9372	5.9357	5.9357
0.2500				
	1	0.9220	0.8835	0.9585
	2	1.9220	1.9047	1.9047
	3	2.9220	2.9142	2.9298
	4	3.9220	3.9185	3.9185
	5	4.9220	4.9204	4.9236
	6	5.9220	5.9213	5.9213

Table 7.1 The Disturbance Spacing $\tilde{\lambda}/\pi$ to Maximize and Minimize the Response to Two Equal Disturbances

	n	1st	2nd	Exact
0.0000				
	1	1.0000	1.0000	1.0000
	2	2.0000	2.0000	2.0000
	3	3.0000	3.0000	3.0000
	4	4.0000	4.0000	4.0000
	5	5.0000	5.0000	5.0000
	6	6.0000	6.0000	6.0000
0.0100				
	1	0.9968	0.9999	0.9937
	2	1.9968	1.9998	1.9998
	3	2.9968	2.9997	2.9939
	4	3.9968	3.9996	3.9996
	5	4.9968	4.9995	4.9941
	6	5.9968	5.9995	5.9995
0.0200				
	1	0.9936	0.9996	0.9877
	2	1.9936	1.9992	1.9992
	3	2.9936	2.9989	2.9884
	4	3.9936	3.9986	3.9986
	5	4.9936	4.9983	4.9890
	6	5.9936	5.9980	5.9980
0.0300				
	1	0.9905	0.9991	0.9818
	2	1.9905	1.9984	1.9984
	3	2.9905	2.9976	2.9832
	4	3.9905	3.9970	3.9970
	5	4.9905	4.9964	4.9845
	6	5.9905	5.9959	5.9959
0.0400				
	1	0.9873	0.9985	0.9760
	2	1.9873	1.9972	1.9972
	3	2.9873	2.9960	2.9785
	4	3.9873	3.9950	3.9950
	5	4.9873	4.9941	4.9805
	6	5.9873	5.9933	5.9933
0.0500				
	1	0.9841	0.9977	0.9704
	2	1.9841	1.9957	1.9957
	3	2.9841	2.9940	2.9741
	4	3.9841	3.9926	3.9926
	5	4.9841	4.9914	4.9768
	6	5.9841	5.9903	5.9903

	n	1st	2nd	Exact
0.0000				
	1	1.0000	1.0000	1.0000
	2	2.0000	2.0000	2.0000
	3	3.0000	3.0000	3.0000
	4	4.0000	4.0000	4.0000
	5	5.0000	5.0000	5.0000
	6	6.0000	6.0000	6.0000
0.0500				
	1	0.9841	0.9977	0.9704
	2	1.9841	1.9957	1.9957
	3	2.9841	2.9940	2.9741
	4	3.9841	3.9926	3.9926
	5	4.9841	4.9914	4.9768
	6	5.9841	5.9903	5.9903
0.1000				
	1	0.9683	0.9915	0.9447
	2	1.9683	1.9852	1.9853
	3	2.9683	2.9807	2.9558
	4	3.9683	3.9774	3.9774
	5	4.9683	4.9749	4.9616
	6	5.9683	5.9731	5.9731
0.1500				
	1	0.9526	0.9823	0.9220
	2	1.9526	1.9713	1.9713
	3	2.9526	2.9643	2.9408
	4	3.9526	3.9599	3.9599
	5	4.9526	4.9572	4.9480
	6	5.9526	5.9555	5.9555
0.2000				
	1	0.9372	0.9711	0.9017
	2	1.9372	1.9554	1.9555
	3	2.9372	2.9470	2.9272
	4	3.9372	3.9424	3.9424
	5	4.9372	4.9400	4.9344
	6	5.9372	5.9387	5.9387
0.2500				
	1	0.9220	0.9584	0.8833
	2	1.9220	1.9389	1.9389
	3	2.9220	2.9298	2.9142
	4	3.9220	3.9256	3.9256
	5	4.9220	4.9236	4.9204
	6	5.9220	5.9228	5.9228

Table 7.2 The Disturbance Spacing $\tilde{\lambda}/\pi$ to Maximize and Minimize the Response to Two Equal and Opposite Disturbances

AN EXPERIMENTAL-ANALYTICAL ROUTINE FOR THE DYNAMIC QUALIFICATION OF AIRCRAFT OPERATING ON ROUGH RUNWAY SURFACES

by

R. Freymann

DFVLR-Institute of Aeroelasticity
Bunsenstraße 10, 3400 Göttingen, Germany

SUMMARY

A mathematical model to be used as a basis for analytical investigations to predict the dynamic structural response of flexible aircraft operating on rough runway surfaces is presented. It is shown how the structural parameters included in the aircraft generalized equations of motion are determined in a ground vibration test on the real aircraft structure and in additional tests on components of the undercarriage. The validation of the developed mathematical model is achieved by a comparison of typical results from frequency response tests and calculations performed on a YF-16 prototype fighter aircraft. Finally, the way in which the developed mathematical model can be used in combination with various systematic test procedures for the dynamic qualification process of aircraft operation on damaged/repaired runways is indicated.

LIST OF SYMBOLS

$\mathbf{A}$		matrix of the factors of a linear combination
$\mathbf{D}$		diagonal matrix of the modal damping factors
F	[N]	force
F_0	[N]	preload force
$\mathbf{K}$		nondiagonal generalized stiffness matrix
$\mathbf{M}$		diagonal generalized mass matrix
Q	[kg m²/s²]	generalized external force
U	[kg m²/s²]	potential of the deformation
V	[m/s]	velocity
W	[kg m²/s²]	kinetic energy
$\mathbf{X}_0$		reference matrix of the unit landing gear elongations
$\mathbf{Z}_0$		matrix of the structural displacements due to a unit reference displacement at the different landing gears
$\mathbf{Z}_{0L}$		diagonal matrix of the unit reference displacements at the landing gears
$\mathbf{c}_L$		diagonal matrix of the (nonlinear) landing gear stiffnesses
$\mathbf{c}_S$		diagonal matrix of the stiffnesses of the ground vibration test suspension system
$\mathbf{c}_T$		diagonal matrix of the (nonlinear) landing gear tire stiffnesses
$\mathbf{d}_L$		diagonal matrix of the (nonlinear) viscous damping factors of the landing gears
$\mathbf{d}_T$		diagonal matrix of the (nonlinear) structural damping factors of the landing gear tires
f	[Hz]	frequency
f_r	[Hz]	eigenfrequency of the r th eigenmode
g		function to describe the geometric nonlinearities of a landing gear
i		imaginary unit
$\mathbf{m}_L$		diagonal matrix of the landing gear unsprung masses
$\mathbf{p}$		vector of the generalized coordinates related to the rough runway profile

$\mathbf{q}$		vector of the generalized coordinates related to global aircraft eigenmodes
q_r		generalized coordinate related to the r-th generalized degree of freedom
$\Delta\mathbf{q}$		vector of the generalized coordinates related to the landing gear (strut) degrees of freedom
t	[sec]	time
x	[m]	structural displacement
$\Delta\mathbf{x}_L$		vector of the landing gear elongations
z	[m]	runway unevenness
Φ		modal matrix
Φ_L		modal matrix of the landing gear displacements
Φ_R		modal matrix related to the rigid-body eigenmodes
ϑ	[% D_{crit}]	structural damping factor
ω	[1/s]	circular frequency
ω_r	[1/s]	circular eigenfrequency of the r-th eigenmode

Indices:

$(\,)_r$	value related to r-th global aircraft eigenmode ($r = 1,2,\ldots,n$)
$(\,)_\mu$	value related to the μ-th landing gear degree of freedom ($\mu = 1,2,\ldots,m$)
$(\,)_T$	value related to a tire parameter
$(\,)_L$	value related to a landing gear parameter
$(\,)_S$	value related to a suspension system parameter
$(\,)_{ST}$	value related to a landing gear strut
$\dot{(\,)}$, $\ddot{(\,)}$	denote first and second derivatives with regard to time

1. INTRODUCTION

For many years, the NATO countries have been dealing with the problem of evaluating the capatibilities of their aircraft to operate from rough runway surfaces. This problem is a primary anticipation in modern warfare tactics, which foresee an early destruction of the opponent's airfields.

To guarantee the readiness of aircraft even in the case of damaged runways, engineers have concentrated on the task of correctly predicting the dynamic structural response of aircraft when taxiing over rough runway surfaces and to establish, based on these data, guidelines (criteria) for the (rapid) repair of damaged runway surfaces.

In order to determine realistic limits of aircraft operational capabilities on the ground, extensive experimental aircraft taxi investigations (Figure 1) have been performed [1,2]. These tests, albeit associated with many difficulties, have proven able to realistically determine the aircraft taxi capabilities on rough surfaces. But since this testing is also very costly, taxi testing will always be restricted to a minimum.

On the other hand, the many analytical investigations performed in the past indicate that, for calculation of realistic dynamic response data, it is necessary to consider in the mathematical

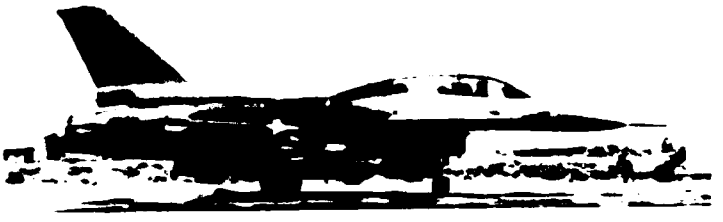

Figure 1: Taxi field testing with F-16 aircraft

model of the aircraft structure, both the aircraft rigid body and flexible eigenmodes as well as the nonlinear and frequency-dependent characteristics of the undercarriage [3]. This requirement is easily formulated, but is more difficult to realize. For the engineer involved in structural dynamics, numerous questions result therefrom, such as how the aircraft structural model should be built in order to allow easy handling of the structural nonlinearities, and how the (modal) parameters of the flexible aircraft structure as well as the characteristics of the undercarriage can be realistically determined.

Closer insight into the overall problem indicates the need to develop a practical mixed experimental-analytical routine which allows experimental determination of realistic structural parameters consistent with a well-adapted mathematical structural model, to be used as a basis in the dynamic response calculations.

This report gives a description of a newly developed experimental-analytical method which can be adopted as a routine in the qualification process of aircraft for its operation on damaged/repaired runways. The practical applicability of the method is demonstrated by the investigations performed on a prototype YF-16 fighter aircraft. In the following chapters and paragraphs, first a model of the aircraft structure is presented. Moreover it is shown how the (structural) parameters included in the aircraft equations of motion can be experimentally determined in various tests performed on the aircraft structure and on its undercarriage. Finally the developed mathematical structural model will be validated by comparing calculated and measured frequency response results of typical structural data.

The work described in this paper was performed by the author at the Air Force Flight Dynamics Laboratory of the Wright-Patterson Air Force Base in Dayton (Ohio) during a one-year stay as "visiting scientist". The author wishes to acknowledge the authorities of the Structures and Dynamics Division for having provided the opportunities to investigate the developed routine on a fighter aircraft of the US Air Force. Gratitude is also due to the many people at the Flight Dynamics Laboratory who graciously provided their support during the various tests.

3. THE AIRCRAFT STRUCTURAL MODEL

The generalized equations of motion of flexible aircraft, as depicted in Figure 2, were derived from the Lagrange Equations [4], which are expressed in the form

$$(1) \qquad \frac{d}{dt}\left(\frac{\partial W}{\partial \dot{q}_r}\right) - \frac{\partial W}{\partial q_r} + \frac{\partial U}{\partial q_r} = Q_r \,, \qquad (r = 1,2,\ldots,n)$$

for a set of n generalized coordinates q_r, related to n generalized degrees of freedom.

Considering n generalized degrees of freedom of the flexible aircraft structure and m additional generalized degrees of freedom for the translatory motion of the undercarriage, the generalized equations of motion of the entire aircraft can be formulated as follows:

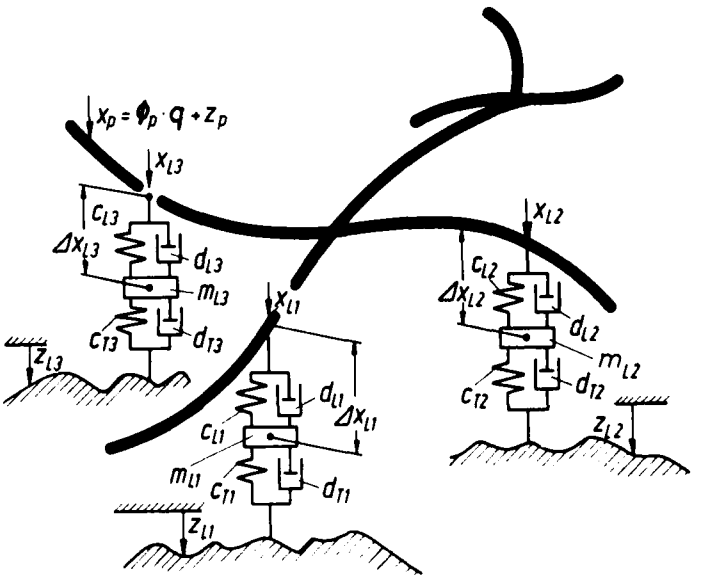

Figure 2: Physical structural aircraft model

$$(2) \qquad \begin{bmatrix} M & \phi_L^T m_L X_0 \\ X_0^T m_L \phi_L & X_0^T m_L X_0 \end{bmatrix} \begin{Bmatrix} \ddot{q}(t) \\ \Delta\ddot{q}(t) \end{Bmatrix} + \begin{bmatrix} 0 & 0 \\ 0 & X_0^T d_L X_0 \end{bmatrix} \begin{Bmatrix} \dot{q}(t) \\ \Delta\dot{q}(t) \end{Bmatrix} + \left[\begin{bmatrix} K + \phi_L^T c_T \phi_L & \phi_L^T c_T X_0 \\ X_0^T c_T \phi_L & X_0^T (c_T + c_L) X_0 \end{bmatrix} + i \begin{bmatrix} D + \phi_L^T d_T \phi_L & \phi_L^T d_T X_0 \\ X_0^T d_T \phi_L & X_0^T d_T X_0 \end{bmatrix} \right] \begin{Bmatrix} q(t) \\ \Delta q(t) \end{Bmatrix} = - \begin{bmatrix} \phi^T m Z_0 + \phi_L^T m_L Z_{0L} \\ X_0^T m_L Z_{0L} \end{bmatrix} \beta(t)$$

with

$$(3) \qquad \Delta \mathbf{x}_L(t) = \mathbf{X}_0 \cdot \Delta \mathbf{q}(t)$$

as the landing gear deformations,

$$(4) \qquad \mathbf{z}_L(t) = \mathbf{Z}_{0L} \cdot \mathbf{p}(t)$$

as the runway roughness encountered by the landing gears, and

$$(5) \qquad \mathbf{z}(t) = \mathbf{Z}_0 \cdot \mathbf{p}(t)$$

as the (rigid-body) displacements at discrete points of the structure induced as the structure encounters runway roughness. At any given time, the total (absolute) displacement at a well-defined point P of the aircraft structure is given by superposition of the elastic and rigid-body mode response and of the forced displacement due to the runway roughness. Thus we can write

$$(6) \qquad x_P(t) = \boldsymbol{\Phi}_P \cdot \mathbf{q}(t) + \mathbf{Z}_{0P} \cdot \mathbf{p}(t) \ , \quad (P = 1,2,\ldots,N) \ .$$

As indicated by Equation (2), consideration of the landing gear degrees of freedom as "additional" degrees of freedom entails that the structural parameters related to the overall elastic aircraft structure are completely separated from the landing gear parameters. This formulation of the equations of motion is advantageous if the dynamic structural parameters of the landing gears have to be modified often during calculation, as for example when nonlinear landing gear characteristics must be considered.

In the following chapters the way in which the various structural parameters included in the generalized equations of motion can be experimentally determined will be shown.

4. GROUND VIBRATION TEST

The aim of a ground vibration test is to provide the modal structural data of a flexible structure. These parameters are

- the eigenfrequencies f_r ,
- the normal mode shapes $\boldsymbol{\Phi}_r$ (eigenmodes),
- the generalized masses M_{rr} ,
- the generalized (modal) damping coefficients D_{rr} .

Common ground vibration test procedures such as the classical "Phase Resonance Method", require the structure to be nearly linear. This is definitely not true for an aircraft structure supported by its undercarriage. Investigating this aircraft structure by a ground vibration test would entail that the measured modal data are a function of the amplitude level of the external excitation applied to the aircraft structure in the test. As a consequence, experimental determination of a set of n o r m a l mode shapes is not possible for this aircraft configuration.

But, if the basic aircraft configuration is modified such that the relative piston motion in the landing gear struts is fully suppressed, i.e. that the landing gear struts are locked, the aircraft structure can be regarded as being nearly linear. The equations of motion of the aircraft configuration with locked landing gear struts can be derived from Equation (2) by setting $\Delta \mathbf{q} = 0$. Moreover it is assumed that, for simulation of the correct boundary conditions in the ground vibration test, the aircraft is supported at its nose and main landing gear tires by a soft (pneumatic) spring system ($c_{S\mu} \ll c_{T\mu}$, $\mu = 1,2,\ldots,m$) with very low damping properties ($d_{S\mu} \to 0$). The YF-16 ground vibration test setup [5] is depicted in Figures 3 and 4 .

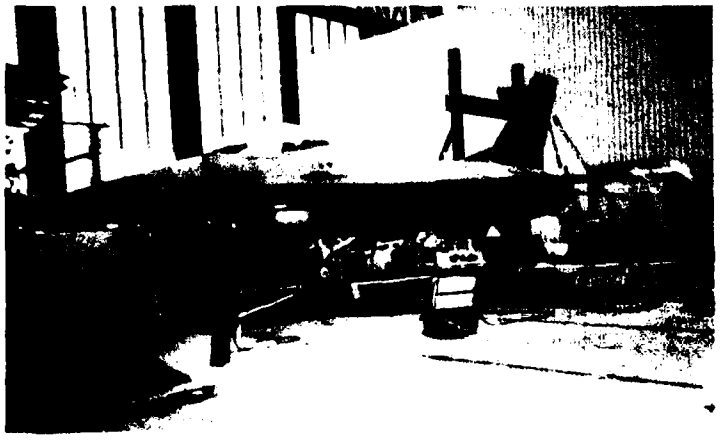

Figure 3: YF-16 ground vibration test setup

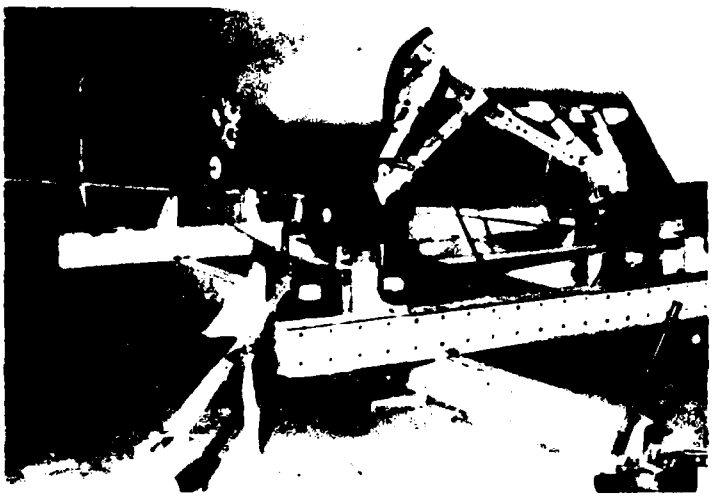

Figure 4: Soft pneumatic suspension system used in the ground vibration test

The condition $c_{S\mu} << c_{T\mu}$ can be easily satisfied when inflating the aircraft tires to a "high" pressure. With $\mathbf{Q}(t)$ as the vector of the generalized external excitation forces, the equations of motion of the aircraft (ground vibration test) configuration with locked landing gears can be formulated as follows:

$$(7) \quad \mathbf{M}\,\ddot{\mathbf{q}}(t) + \left[\left[\mathbf{K} + \boldsymbol{\Phi}_L^T\,\mathbf{c}_S\,\boldsymbol{\Phi}_L\right] + i\left[\mathbf{D} + \boldsymbol{\Phi}_L^T\,\mathbf{d}_T\,\boldsymbol{\Phi}_L\right]\right]\mathbf{q}(t) = \mathbf{Q}(t) .$$

Application of the classical phase resonance ground vibration test method [6] to this system allows the eigenfrequencies f_r, the generalized masses M_{rr} (Table 1) and the normal mode shapes $\boldsymbol{\Phi}_r$ (Figures 5 and 6) to be determined directly.

MODE	EIGENFREQUENCY f_r [Hz]	GENERALIZED MASS M_{rr} [kg m²]	DAMPING COEFFICIENT ϑ_r [% D_{crit}]
RB 1: Rigid Body Pitch	0.621	1890.0	/
RB 2: Rigid Body Heave	1.410	4611.0	/
RB 3: Rigid Body Roll	2.019	106.0	/
S 1 : Symm. Bending	4.62	870.0	1.6
S 2 : Symm. Missile Pitch	7.01	275.0	1.5
S 3 : Fuselage Vert. Bending	12.19	317.0	1.7
A 1 : Asymm. Missile Pitch	5.73	1186.0	1.7
A 2 : Asymm. Wing Bending	8.21	346.0	1.4
A 3 : Fin Bending	14.10	33.2	1.9
A 4 : Fuselage Lat. Bending	16.77	110.0	1.7

Table 1: Modal parameters of YF-16 aircraft

The values of the modal damping coefficients are fixed or derived as follows:

$$D_{rr} \equiv 0 \qquad \text{for all rigid-body modes}$$

and

$$D_{rr} \approx D_{rr} + \left[\boldsymbol{\Phi}_L^T\,\mathbf{d}_T\,\boldsymbol{\Phi}_L\right]_{rr} = \frac{2\,\vartheta_r \cdot \omega_r^2\,M_{rr}}{100}$$

for the flexible modes, ϑ_r being the experimentally determined modal damping coefficients, as denoted in Table 1. This approximation of the structural damping is permissible, since the values of the coefficients in $\boldsymbol{\Phi}_L$ are small relative to flexible eigenmodes.

The coefficients of the (nondiagonal) stiffness matrix $\mathbf{K}$ are determined from

$$(8) \qquad \mathbf{K} = \left[\omega_r^2\,M_{rr}\right] - \boldsymbol{\Phi}_L^T\,\mathbf{c}_S\,\boldsymbol{\Phi}_L$$

which is possible when the stiffnesses $c_{S\mu}$ of the aircraft suspension system are known. Determination of these stiffnesses can easily be achieved in a static loading test (Table 2).

Thus, after completion of the ground vibration test, the following parameters are available:

- the diagonal generalized mass matrix $\mathbf{M}$,
- the diagonal modal damping matrix $\mathbf{D}$,

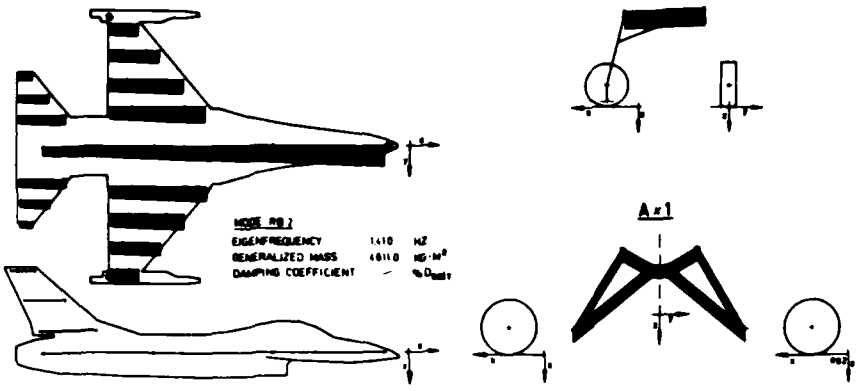

Figure 5: Rigid-body heave mode

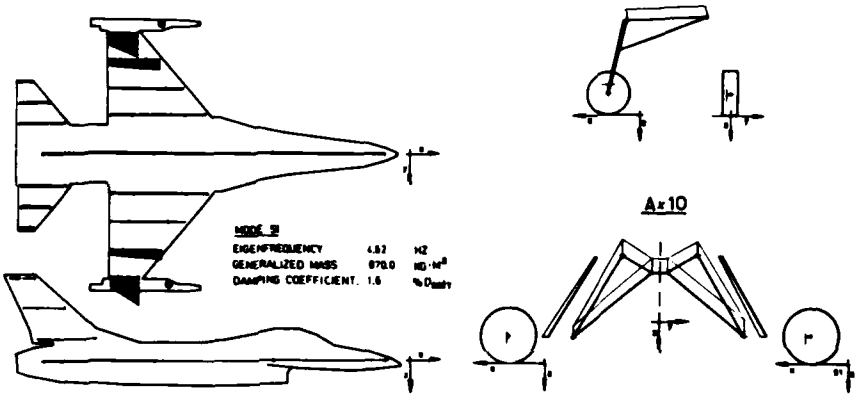

Figure 6: First symmetric wing bending mode

Nose LG*)	Left Main LG*)	Right Main LG*)
$c_{S1} = 1.34 \cdot 10^5$ N/m	$c_{S2} = 1.56 \cdot 10^5$ N/m	$c_{S3} = 1.50 \cdot 10^5$ N/m

*) Landing gear

Table 2: Measured stiffnesses of the YF-16 ground vibration test suspension system

- the nondiagonal generalized stiffness matrix $\mathbf{K}$,
- the modal matrix Φ and its submatrix Φ_L,
- the diagonal matrix $\mathbf{c}_S$ containing the suspension stiffnesses.

A review of the equations of motion of aircraft with unlocked landing gears (Equation (2)) indicates that all parameters related to the overall flexible aircraft structure can be determined from the ground vibration test investigations as described. The remaining unknown (nonlinear) parameters are all related to the undercarriage. Experimental determination of these parameters in additional tests, performed on the landing gear struts and tires will be demonstrated in the following two chapters.

5. LANDING GEAR STRUT TEST

A major problem encountered when performing dynamic aircraft taxi response calculations is how to obtain realistic data for approximation of the spring/damper characteristics of the landing gear (strut) elements. Usually the required data are not available, since the investigations performed by the landing gear manufacturer normally concentrate on (transient) landing gear drop tests for simulation of the landing impact.

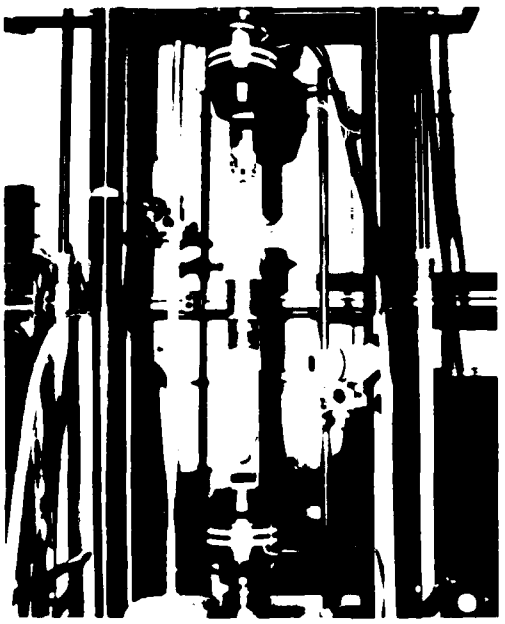

Figure 7: YF-16 main landing gear strut test setup

For the performance of dynamic response calculations, however, we need to know the dynamic stiffness and damping characteristics of the landing gear strut elements. These characteristics can be determined by (harmonically) cycling the landing gear strut in a testing machine (Figure 7) at various frequencies and amplitudes of its displacement. To obtain correct landing gear data for various aircraft gross weights, the landing gear strut tests must be performed at different levels of the static strut preload force.

For a strut preload force $F_0 = 75$ kN, consistent with the static loading of the strut installed in the aircraft in the case of the YF-16 configuration, cycling tests were performed on a two-stage main landing gear strut. The experimentally determined values of the (equivalent) dynamic stiffness [7] are depicted in Figure 8. The plotted curves indicate a strong nonlinear but a nearly frequency-independent behavior of the dynamic strut stiffness. Figure 9 depicts, at a frequency of 1 Hz, the equivalent stiffness c_{ST} of the strut as a function of the amplitude of vibration x.

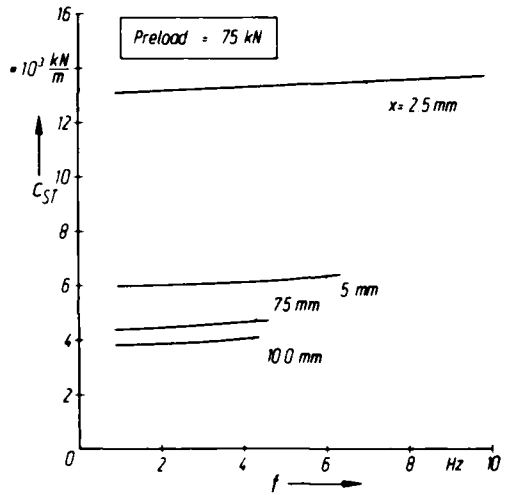

Figure 8: Experimentally determined nonlinear stiffness behavior of the YF-16 main landing gear strut

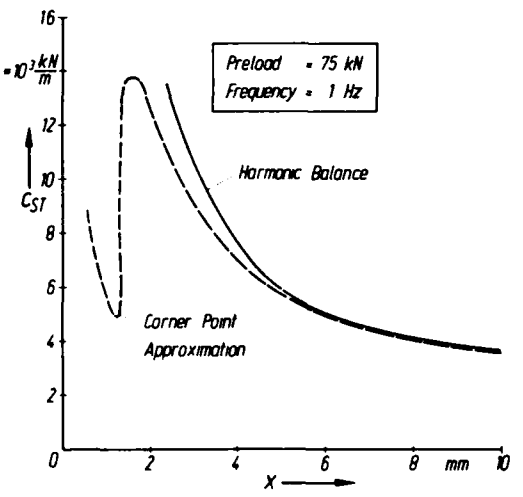

Figure 9: Experimentally determined equivalent dynamic stiffness of the YF-16 main landing gear strut

The dynamic damping characteristics of the strut were obtained from measured hysteresis curves [8], some of which are depicted in Figure 10. A graph of the viscous damping factor d_{ST} is shown in Figure 11, indicating a strong nonlinear and frequency-dependent damping behavior of the strut.

The thus determined strut characteristics $c_{ST\mu}$ and $d_{ST\mu}$ ($\mu = 1,\ldots,m$) are not identical to the landing gear characteristics $c_{L\mu}$ and $d_{L\mu}$ considered in Equation (2). But their respective values are interrelated by a factor or a nonlinear function $g_\mu = g_\mu(\Delta x_{L\mu})$, which can be derived from the landing gear geometry. The following interrelations exist:

(9a) $$c_{L\mu} = c_{ST\mu} \cdot g_\mu \quad \text{(geometry)}, \qquad (\mu = 1,\ldots,m) \ .$$

(9b) $$d_{L\mu} = d_{ST\mu} \cdot g_\mu \quad \text{(geometry)},$$

Thus, after performance of the landing gear strut tests, the following data are available:

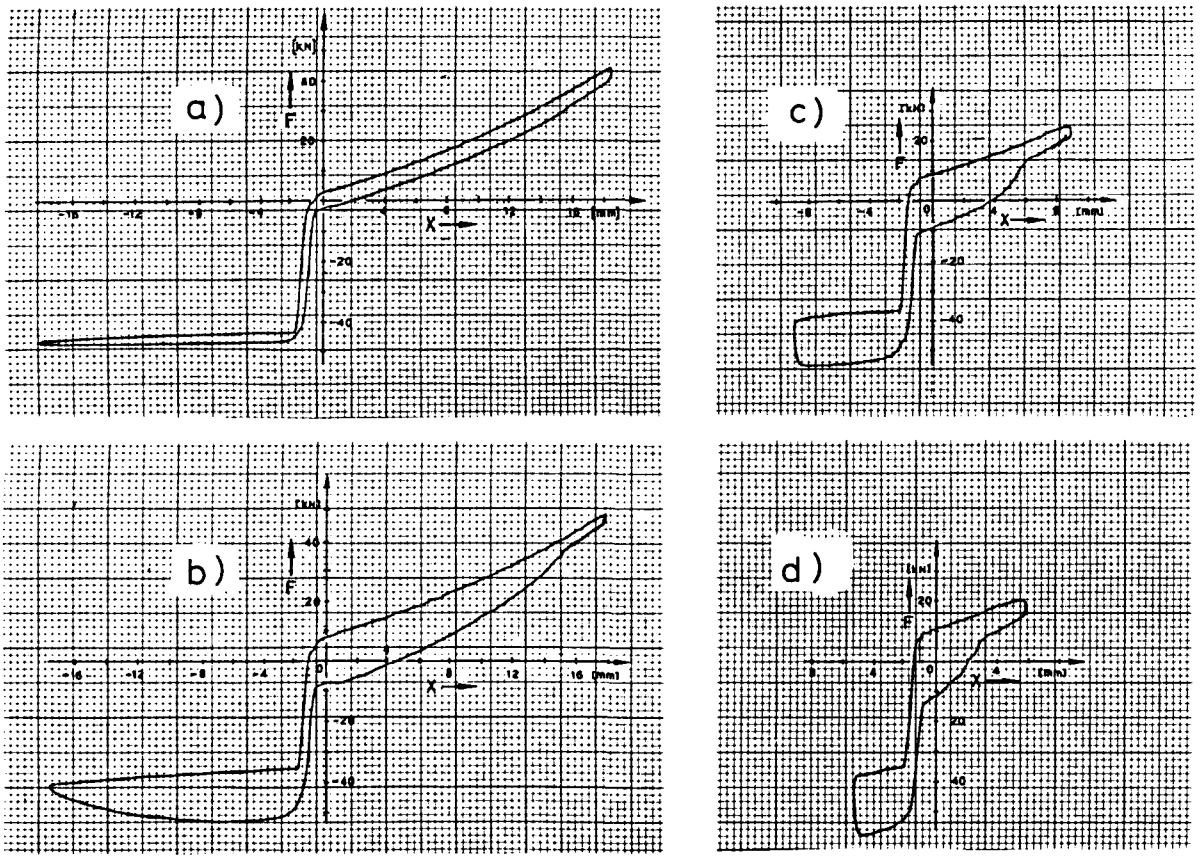

Figure 10: Measured hysteresis curves on the YF-16 main landing gear strut at a static preload of 75 kN
a) f = 0.25 Hz b) f = 1.0 Hz c) f = 3.0 Hz d) f = 5.0 Hz

- the landing gear stiffness characteristics

$$c_{L\mu} = c_{L\mu}(F_{0\mu}, f, \Delta x_{L\mu}), \quad (\mu = 1,\ldots,m)$$

and

- the landing gear (viscous) damping characteristics

$$d_{L\mu} = d_{L\mu}(F_{0\mu}, f, \Delta x_{L\mu}), \quad (\mu = 1,\ldots,m) .$$

Discrete values of these different characteristics are the coefficients of the diagonal matrices $\mathbf{c}_L$ and $\mathbf{d}_L$, respectively. With regard to evaluating the coefficients of the landing gear mass matrix $\mathbf{m}_L$ it has to be mentioned that their determination is of no difficulty, since the values of the unsprung masses $m_{L\mu}$ ($\mu = 1,\ldots,m$) are exactly known by the manufacturer.

6. TIRE TEST

To obtain realistic tire stiffness and damping data, tests must be performed on spinning tires. Dynamic tire stiffness and damping data can be experimentally determined in a test setup, as depicted in Figure 12. The operation of the test setup is as follows:

The runway surface is simulated by the rolling surface of a wheel, spinning at a high angular velocity and driving the aircraft tire. A hydraulic shaker (harmonically) cycles the tire

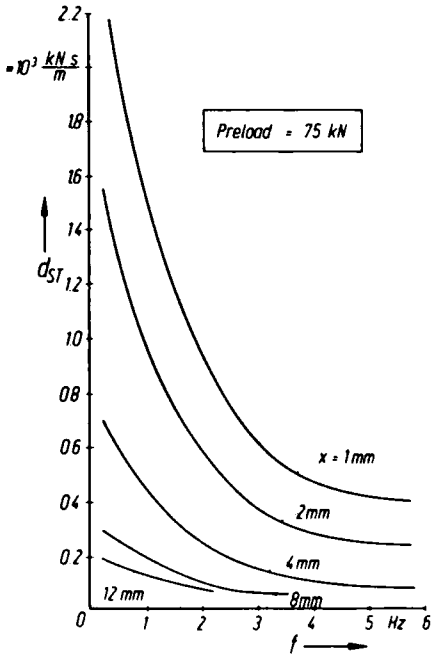

Figure 11: Experimentally determined viscous damping factor of the YF-16 main landing gear strut

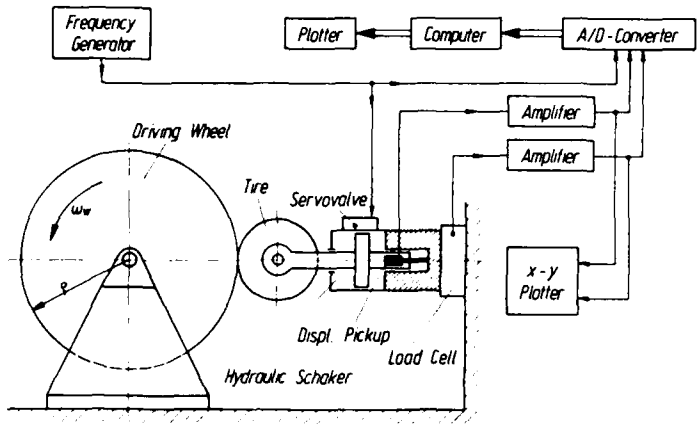

Figure 12: Setup for dynamic tire testing

on the wheel. Tests are performed at various wheel speeds $V = \omega_W \cdot \rho$, various static tire preloads F_0 and for various frequencies f and amplitudes x of the dynamic shaker excitation. Measuring the dynamic force F and the corresponding displacement x, allows determination of the tire stiffness characteristic

$$c_T = F/x = c_T(F_0, V, f, x)$$

measurement of hysteresis curves allows determination of the tire structural damping characteristics

$$d_T = d_T(F_0, V, f, x)$$

Discrete values of the $c_{T\mu}$ and $d_{T\mu}$ characteristics ($\mu = 1,\ldots,m$), determined for the different tires of the nose and main landing gear are entered as coefficients into the diagonal matrices $\mathbf{c}_T$ and $\mathbf{d}_T$, respectively. Thus, after completion of the tire tests, the matrices $\mathbf{c}_T$ and $\mathbf{d}_T$ are well defined.

Within the scope of the investigations performed on the YF-16 aircraft, tests were only carried out on the non-spinning tires of the nose and main landing gears. The investigations concentrated on the determination of

- the (nonlinear) load/stroke tire characteristics from which the (nonlinear) stiffness characteristic can be derived,
- (quasi-static) tire hysteresis curves for evaluation of the structural tire damping.

For performance of the tests, the different tires were squeezed in a testing machine (Figure 13). As a typical result, Figure 14 depicts the static load/stroke curve of the main landing gear tire. It can be noticed that, at higher preloads, the tire stiffness is nearly a constant. Tire nonlinearities are of secondary importance when compared to the highly nonlinear behavior of the landing gear struts. But, should the tire load/stroke curve indicate larger nonlinearities, the methods described in [7] can be used for de-

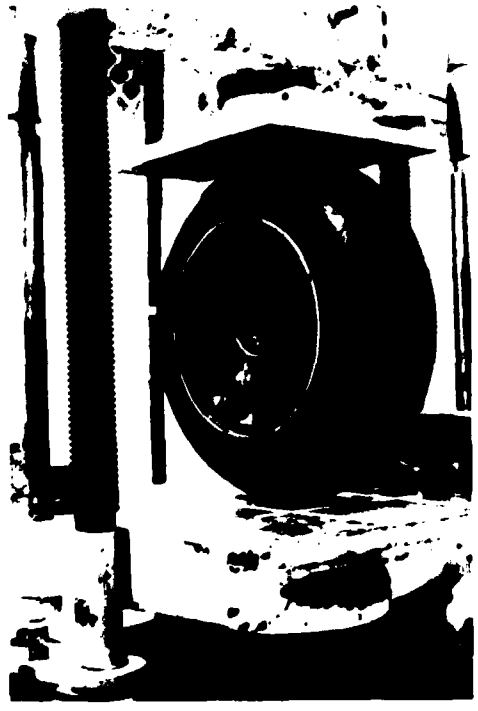

Figure 13: Machine used for the static and quasi-static tire testing

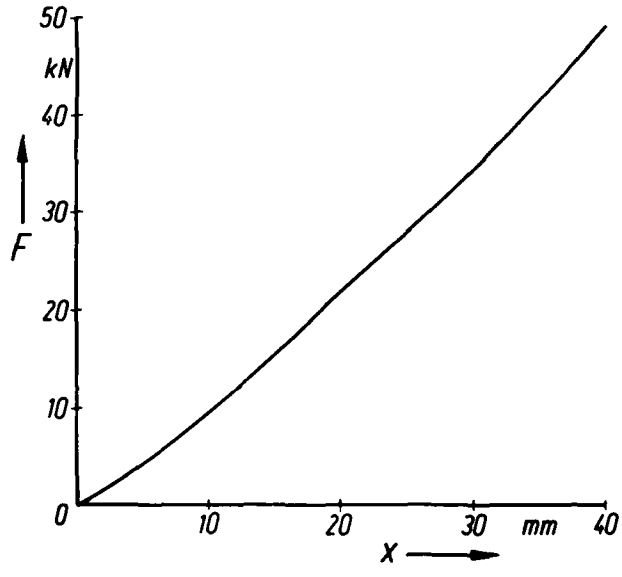

Figure 14: Measured load/stroke curve of a YF-16 main landing gear tire

termination of an equivalent amplitude-dependent stiffness $c_T = c_T(F_0, x)$. Figure 15 shows hysteresis curves measured around a fixed static tire preload $F_0 = 30$ kN. From the hysteresis curves, an average structural damping value of 5 % D_{crit} was determined.

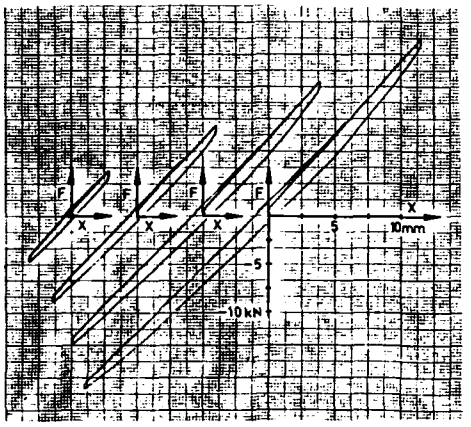

Figure 15: Measured hysteresis curves on the YF-16 main landing gear tire at a static preload of 30 kN

7. DYNAMIC RESPONSE INVESTIGATIONS

As all structural parameters denoted at the left-hand side of Equation (2) are known after completion of the ground vibration, landing gear strut and tire tests, dynamic response calculations can be performed for a well-defined runway roughness input, provided the matrix at the right-hand side of the equation system is known. At first it seems that the discrete (finite element) mass matrix of the aircraft structure must be known for determination of the right-hand submatrix $[\boldsymbol{\Phi}^T \mathbf{m} \mathbf{Z}_0 + \boldsymbol{\Phi}_L^T \mathbf{m}_L \mathbf{Z}_{0L}]$. This "problem" can be avoided when writing the matrix of displacements $\mathbf{Z}_0$ in a series, as a superposition of the rigid-body mode displacements $\boldsymbol{\Phi}_R$ determined in the ground vibration test, as follows:

$$\mathbf{Z}_0 = \boldsymbol{\Phi}_R \cdot \mathbf{A} \quad , \tag{10}$$

the coefficients of matrix $\mathbf{A}$ being the factors of the linear combination. Considering the existing orthogonality relations between the (measured) eigenmodes, we can write:

$$[\boldsymbol{\Phi}^T \mathbf{m} \mathbf{Z}_0 + \boldsymbol{\Phi}_L^T \mathbf{m}_L \mathbf{Z}_{0L}] = \begin{bmatrix} \mathbf{M} \\ \hline 0 \end{bmatrix} \cdot \mathbf{A} \quad , \tag{11}$$

$\mathbf{M}$ being the diagonal generalized mass matrix, as defined at the left-hand side of Equation (2). The coefficients of matrix $\mathbf{M}$ have been determined in the ground vibration test. Equation (11) indicates that there is no direct external excitation in the elastic aircraft eigenmodes by the runway roughness. The elastic modes are all excited by their respective rigid-body/elastic mode coupling terms at the left-hand side of Equation (2).

7.1 Dynamic Response Testing with AGILE

By virtue of the Aircraft Ground Induced Loads Excitation (AGILE) shaker test facility (Figure 16) now available at the Air Force Flight Dynamics Laboratory at Wright-Patterson Air Force Base in Dayton (Ohio), extensive dynamic response testing on real aircraft structures has become possible [9]. This facility allows performance of special investigations which could not be realized in the past. For instance it is possible to harmonically excite the aircraft via its tires up to frequencies in the vicinity of 30 Hz and to perform tests in a locked landing gear aircraft configuration. These possibilities first seem to be of no importance since neither this type of excitation nor this configuration are representative. With regard to the qualification of the aircraft structural model, however, this special type of testing is advantageous.

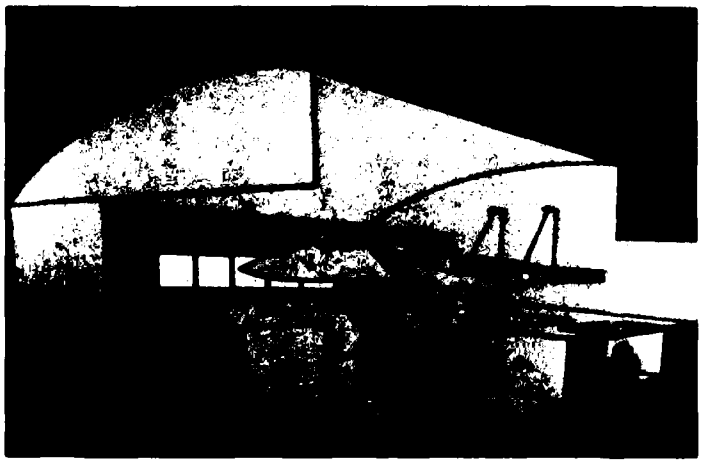

Figure 16: The AGILE shaker test facility

First, excitation of the structure by a (swept) sine forcing function allows excitation of all eigenmodes in the frequency range of interest. A comparison between measured and calculated frequency response data (transfer functions) clearly

indicates which of the modes are correctly modelled and which are not. Secondly, the ability to test the aircraft in its locked landing gear configuration allows verification of whether the flexible aircraft structure itself - without consideration of the dynamically very complicated landing gear - has been modelled correctly. This intermediate verification step is important in a response analysis, since there definitely has to be agreement between measured and calculated data for the aircraft locked landing gear configuration b e f o r e concentrating on the far more problematic (real) configuration with unlocked landing gear struts.

A survey of the experimental and analytical investigations performed on the YF-16 aircraft in both of the configurations with locked and unlocked landing gear struts is given in the next two sections.

7.2 Locked Landing Gear Configuration

A full description of the AGILE frequency response tests performed on the YF-16 aircraft (Figure 17) is given in [10]. Aircraft response data were recorded and analyzed for a series of different shaker excitation configurations, e.g. excitation of the aircraft at the nose or main landing gear tires only or simultaneous excitation at both of the landing gear systems. The aircraft was excited by the shakers with a constant amplitude swept sine signal in the frequency range from 0.6 to 15 Hz. Plots of typical dynamic response data, resulting from a test with simultaneous excitation of the nose and main landing gear tires, are plotted as dashed curves in Figures 18 to 21. Moreover these plots depict the corresponding results from dynamic response calculations based on Equation (2) with consideration of $\Delta \mathbf{q} \equiv 0$. Only symmetric

Figure 17: AGILE testing on the YF-16 aircraft

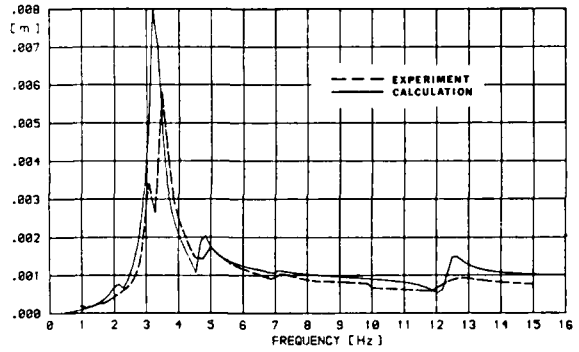

Figure 18: Main landing gear tire deformation

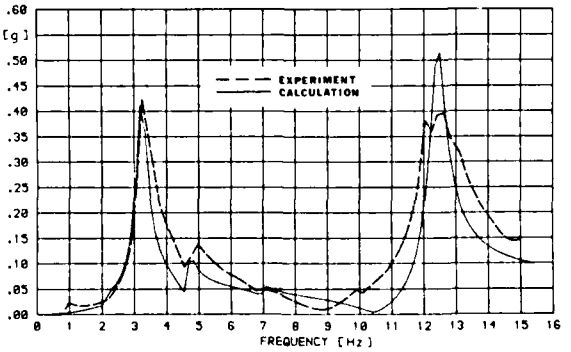

Figure 19: Acceleration at the nose landing gear tire axle

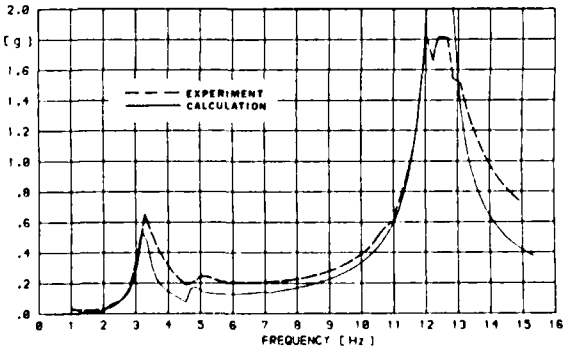

Figure 20: Acceleration at the fuselage nose

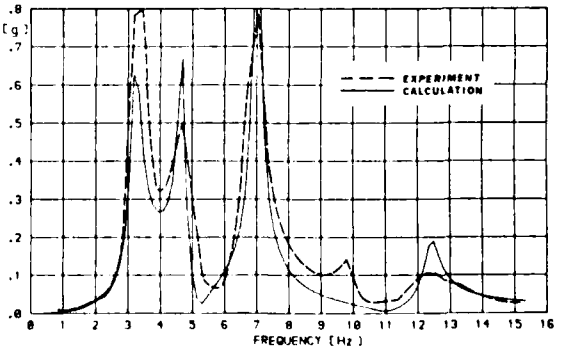

Figure 21: Acceleration at the left wing tip

aircraft eigenmodes were taken into account in the calculations, i.e. the modes RB1, RB2, S1, S2 and S3 of Table 1. All calculations were performed on the basis of the true measured structural data, with no updating of any of the structural parameters with regard to an improvement of the calculated results.

The figures indicate good overall agreement between measured and calculated data. Especially the frequencies of the modes are well determined by the calculation. Some discrepancies between the amplitude data are due to the "bad" resolution (0.15 Hz interval between frequency steps) of the digital Fast Fourier Transform Analyzer used in the data reduction process. The broader "peaks" measured in some responses (e.g. in the 12.5 Hz mode of Figure 20) are probably due to a nonlinear behavior of the aircraft structure which was excited at real high g-levels during the response tests.

In general, the agreement between measured and calculated response data was found to be accurate enough to start the dynamic response calculations on the aircraft configuration with unlocked landing gear struts.

7.3 Configuration with Unlocked Landing Gear Struts

Analogous to the procedure described in Section 7.2, experimental and analytical frequency response investigations were performed on the YF-16 aircraft in its (normal) unlocked landing gear configuration. Figures 22 to 25 depict typical frequency response data for the same shaker excitation configuration as investigated in Section 7.2, but for a higher amplitude level of the excitation. In the calculations the experimentally determined nonlinear landing gear characteristics were considered.

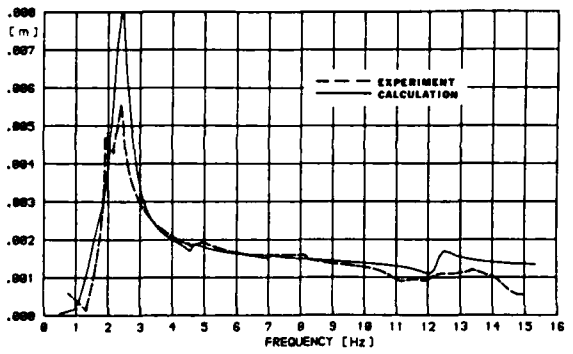

Figure 22: Nose landing gear strut deformation

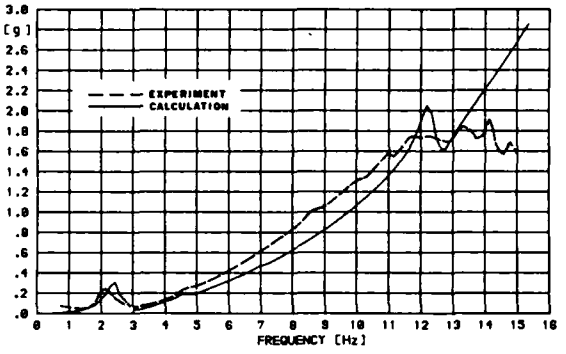

Figure 23: Acceleration at the main landing gear tire axle

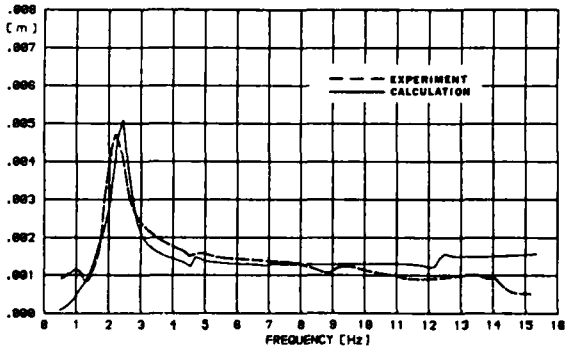

Figure 24: Main landing gear strut deformation

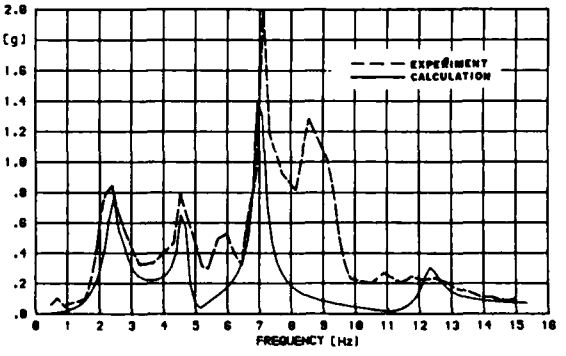

Figure 25: Acceleration at the left wing tip

The figures show that there is reasonable agreement between calculated and measured results. Except in case of the acceleration value, depicted in Figure 25, the correlation cannot be regarded as satisfactory. The discrepancy between measured and calculated curves in this plot is mainly due to the fact that two asymmetric modes (at 6 and 8.5 Hz) are excited by the symmetric shaker excitation. While performing subsequent tests on the landing gears, it was noticed that this effect has to be attributed to the different transfer behavior of the left and right main landing gear struts.

8. CONCLUSION

The many investigations described in this report have shown that the dynamic (frequency) structural response of aircraft to an external excitation at its landing gear tires can be correctly calculated. To obtain satisfactory results, however, it is required that the mathematical model of the aircraft structure be carefully adapted to a series of tests allowing experimental determination of all structural parameters included in the generalized equations of motion. It was noted that especially the nonlinear-, frequency- and preload-dependent characteristics of the undercarriage have to be carefully considered in the calculations.

Despite the extensive investigations already performed, further effort is required for the developed mathematical model to be used in time domain analyses allowing the prediction of the aircraft structural response to a (discrete) runway roughness, e.g. bumps, repairs. But the entire philosophy of aircraft testing, as described in this paper, in combination with the developed mathematical structural model can be used as a basis for a routine allowing dynamic qualification of aircraft for operation on damaged/repaired runways. Figure 26 depicts in a block diagram the entire qualification process consisting of a series of systematic analytical and test investigations. The routine makes ample use of the AGILE shaker system as a qualification test setup. For the validation of the mathematical structural model it is considered to be of importance to perform AGILE tests on both of the aircraft configurations with locked and unlocked landing gear struts. But since AGILE cannot simulate spinning tire effects, this facility does not have the capability to fully replace the taxi field tests. Taxi field tests on real aircraft will remain necessary to completely demonstrate the aircraft operational capabilities on the ground.

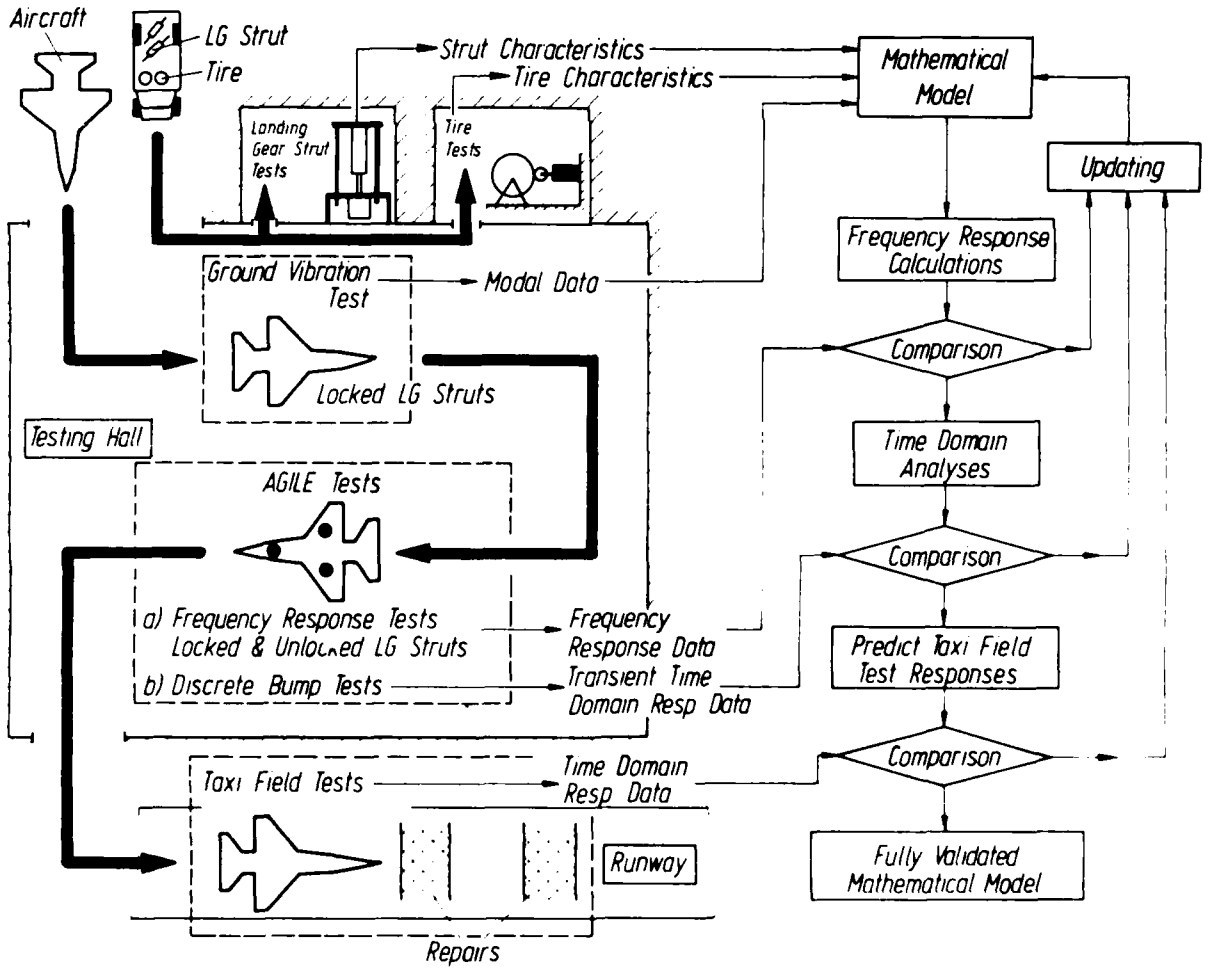

Figure 26: Block diagram of the aircraft qualification routine

9. REFERENCES

[1] HOLPP, J.E.:
The 'Have Bounce' Program. AGARD-CP-326 (1982).

[2] OTTENS, H.H.:
Predicted and Measured Landing Gear Loads for the NF-5 Aircraft Taxiing over a Bumpy Runway. AGARD-CP-326 (1982).

[3] KRAUSS, A.; BARTSCH, O.; KEMPF, G.:
Parameters Affecting Aircraft Performance on Runways in Bad Condition. AGARD-R-685 (1979).

[4] FÖRSCHING, H.:
Grundlagen der Aeroelastik. Springer-Verlag, Berlin/Heidelberg/New York (1974).

[5] FREYMANN, R.:
YF-16 Ground Vibration Test. AFWAL-TM-84-173-FIBEB (1984).

[6] BREITBACH, E.:
A Semi-Automatic Modal-Survey Test Technique for Complex Aircraft and Spacecraft Structures. ESRO-SP-99 (1973).

[7] FREYMANN, R.:
Linearization Techniques. AFWAL-TM-84-229-FIBEB (1984).

[8] THOMSON, W.T.:
Theory of Vibration. Prentice-Hall, Inc. Englewood Cliffs (New Jersey).

[9] JOHNSON, W.P.; FREYMANN, R.; OLSEN, J.J.:
The Agile Test Facility to Evaluate the Readiness of Fighter Aircraft to Operate on Rough/Damaged/Repaired Airfields. Paper presented at the Aircraft Structural Integrity Conference. Macon (Georgia) 27-29, Nov. 1984.

[10] FREYMANN, R.:
Frequency Response Tests Performed on a YF-16 Aircraft Using the AGILE Test Facility. AFWAL-TM-84-205-FIBEB (1984).

REPORT DOCUMENTATION PAGE

1. Recipient's Reference	2. Originator's Reference	3. Further Reference	4. Security Classification of Document
	AGARD-R-739	ISBN 92-835-0409-7	UNCLASSIFIED

5. Originator Advisory Group for Aerospace Research and Development
North Atlantic Treaty Organization
7 rue Ancelle, 92200 Neuilly sur Seine, France

6. Title

AIRCRAFT DYNAMIC RESPONSE TO DAMAGED AND REPAIRED RUNWAYS

7. Presented at

the 61st Meeting of the Structures and Materials Panel of AGARD in Oberammergau, Germany, 8—13 September 1985.

8. Author(s)/Editor(s)	9. Date
Various	March 1987
10. Author's/Editor's Address	**11. Pages**
Various	44

12. Distribution Statement This document is distributed in accordance with AGARD policies and regulations, which are outlined on the Outside Back Covers of all AGARD publications.

13. Keywords/Descriptors

Military aircraft	Undercarriage
Landing gear	Impact shock
Airframes	Runways
Aircraft landing	

14. Abstract

This report contains two papers on the dynamic response of aircraft operating from damaged and repaired runways. In the first paper the response of a simplified representation of an aircraft to two discrete disturbances is analysed to see how the second disturbance modifies system behaviour caused by the first disturbance. The second paper provides a mathematical model which can be used for calculation of the dynamic response of aircraft structures operating on rough surfaces; a comparison is made between theoretical predictions for a YF16 aircraft and typical measurements from frequency response tests.

AGARD Report No.739
Advisory Group for Aerospace Research and Development, NATO
AIRCRAFT DYNAMIC RESPONSE TO DAMAGED AND REPAIRED RUNWAYS
Published March 1987
44 pages

This report contains two papers on the dynamic response of aircraft operating from damaged and repaired runways. In the first paper the response of a simplified representation of an aircraft to two discrete disturbances is analysed to see how the second disturbance modifies system behaviour caused by the first disturbance. The second paper provides a mathematical model which can be used for calculation of the dynamic response of aircraft

P.T.O

AGARD-R-739

Military aircraft
Landing gear
Airframes
Aircraft landing
Undercarriage
Impact shock
Runways

AGARD Report No.739
Advisory Group for Aerospace Research and Development, NATO
AIRCRAFT DYNAMIC RESPONSE TO DAMAGED AND REPAIRED RUNWAYS
Published March 1987
44 pages

This report contains two papers on the dynamic response of aircraft operating from damaged and repaired runways. In the first paper the response of a simplified representation of an aircraft to two discrete disturbances is analysed to see how the second disturbance modifies system behaviour caused by the first disturbance. The second paper provides a mathematical model which can be used for calculation of the dynamic response of aircraft

P.T.O

AGARD-R-739

Military aircraft
Landing gear
Airframes
Aircraft landing
Undercarriage
Impact shock
Runways

AGARD Report No.739
Advisory Group for Aerospace Research and Development, NATO
AIRCRAFT DYNAMIC RESPONSE TO DAMAGED AND REPAIRED RUNWAYS
Published March 1987
44 pages

This report contains two papers on the dynamic response of aircraft operating from damaged and repaired runways. In the first paper the response of a simplified representation of an aircraft to two discrete disturbances is analysed to see how the second disturbance modifies system behaviour caused by the first disturbance. The second paper provides a mathematical model which can be used for calculation of the dynamic response of aircraft

P.T.O

AGARD-R-739

Military aircraft
Landing gear
Airframes
Aircraft landing
Undercarriage
Impact shock
Runways

structures operating on rough surfaces; a comparison is made between theoretical predictions for a YF16 aircraft and typical measurements from frequency response tests.

Papers presented at the 61st Meeting of the Structures and Materials Panel of AGARD in Oberammergau, Germany, 8—13 September 1985.

ISBN 92-835-0409-7

structures operating on rough surfaces; a comparison is made between theoretical predictions for a YF16 aircraft and typical measurements from frequency response tests.

Papers presented at the 61st Meeting of the Structures and Materials Panel of AGARD in Oberammergau, Germany, 8—13 September 1985.

ISBN 92-835-0409-7

structures operating on rough surfaces; a comparison is made between theoretical predictions for a YF16 aircraft and typical measurements from frequency response tests.

Papers presented at the 61st Meeting of the Structures and Materials Panel of AGARD in Oberammergau, Germany, 8—13 September 1985.

ISBN 92-835-0409-7

structures operating on rough surfaces; a comparison is made between theoretical predictions for a YF16 aircraft and typical measurements from frequency response tests.

Papers presented at the 61st Meeting of the Structures and Materials Panel of AGARD in Oberammergau, Germany, 8—13 September 1985.

ISBN 92-835-0409-7

END

7-87

DTIC